Iranian Journal of Science and Technology, Transactions of Civil Engineering
https://doi.org/10.1007/s40996-024-01482-x

RESEARCH PAPER

A New Higher-Order Finite Element Model for Free Vibration and Buckling of Functionally Graded Sandwich Beams with Porous Core Resting on a Two-Parameter Elastic Foundation Using Quasi-3D Theory

Ibrahim Mohamed[1] · Volkan Kahya[1] · Sebahat Şimşek[1]

Received: 1 February 2024 / Accepted: 18 May 2024

Abstract

In this paper, a new higher-order finite element model is proposed for free vibration and buckling analysis of functionally graded (FG) sandwich beams with porous core resting on a two-parameter Winkler-Pasternak elastic foundation based on quasi-3D deformation theory. The material properties of FG sandwich beams vary gradually through the thickness according to the power-law distribution. The governing equation of motion is derived from the Lagrange's equations. Three different porosity patterns including uniform, symmetric, and asymmetric are considered. The accuracy and convergence of the proposed model are verified with several numerical examples. A comprehensive parametric study is carried out to explore the effects of the boundary conditions, skin-to-core thickness ratio, power-law index, slenderness, porosity coefficient, porous distribution of the core, and elastic foundation parameters on the natural frequencies and critical buckling loads of FG sandwich beams.

Keywords FG sandwich beam · Quasi-3D theory · Elastic foundation · Porosity · Free vibration · Buckling · Finite element method

1 Introduction

Functionally graded porous materials (FGPMs) are a new emerging class of functionally graded materials (FGMs) that have gained considerable interest due to their distinctive composition and properties. In addition to gradual variation in the material properties of conventional FGMs, these materials introduce porosity as an additional variable to the material gradient. Beyond sharing the common advantages of conventional FGMs, their lightweight nature, high strength, enhanced energy absorption capabilities, and improved thermal and acoustic insulation properties have driven the development of functionally graded sandwich structures with FG porous core (Bang and Cho 2015; Conde et al. 2006; Betts 2012). With their potential for improved performance and durability, these structures in various forms such as beams, plates, and shells have found potential applications in a variety of engineering fields (Magnucka-Blandzi and Magnucki 2007; Patel et al. 2018; Smith et al. 2012).

Numerous researchers have performed extensive studies to emphasize the mechanical behaviors of FGP sandwich beams using various theories and solution methods (Han et al. 2012; Wu et al. 2020; Lefebvre et al. 2008). A variety of theories available to analyze FGP sandwich beams can be classified mainly as classical beam theory (CBT), first-order shear deformation theory (FSDT), higher-order shear deformation theories (HSDT), and quasi-3D deformation theory. Tang et al. (2018) conducted linear and nonlinear buckling analysis of porous beams based on Euler Bernoulli beam theory. Wattanasakulpong and Ungbhakorn (2014) employed CBT to assess both the linear and nonlinear vibrations of FGP beams. Eltaher et al. (2018) used CBT to investigate the bending and vibration behavior of porous nanobeams. Turan et al. (2023) used the

✉ Volkan Kahya
volkan@ktu.edu.tr

Ibrahim Mohamed
higiloita6@gmail.com

Sebahat Şimşek
sebahatkaraca@ktu.edu.tr

1 Faculty of Engineering, Department of Civil Engineering, Karadeniz Technical University, 61080 Trabzon, Turkey

Published online: 04 June 2024

Ritz method, finite element method (FEM), and artificial neural networks (ANNs) based on FSDT to investigate the free vibration and buckling behavior of FG porous beams under various boundary conditions.

Using FSDT, Chen et al. (2016) investigated the nonlinear free vibration of sandwich beams with an FG porous core. Chen et al. (2015) explored the buckling and bending of FG porous Timoshenko beams. Bamdad et al. (2019) investigated the vibration and buckling behavior of a sandwich Timoshenko beam with a porous core. Grygorowicz et al. (2015) conducted the buckling analysis of a sandwich beam with an FG porous core using FSDT. Alambeigi et al. (2020) investigated the free and forced vibration characteristics of a sandwich beam with an FG porous core and composite face layers embedded with shape memory alloy via FSDT.

Derikvand et al. (2023) studied the buckling of FG sandwich beams with porous ceramic core using HSDT. Ramteke and Panda (2021) examined the free vibrations of a multi-directional FG structure considering the influences of variable grading and porosity distribution with HSDT. Hung and Truong (2018) investigated the free vibration response of sandwich beams with an FG porous core resting on a Winkler elastic foundation using various shear deformation theories. Nguyen et al. (2022a) proposed a two-variable shear deformation theory to investigate the buckling, bending, and vibration characteristics of FGP beams considering various porosity distribution patterns. Srikarun et al. (2021) used Reddy's third-order shear deformation theory to examine the linear and nonlinear bending analysis of sandwich beams with FG porous core under various types of distributed loads. Nguyen et al. (2023) developed a Legendre-Ritz approach to investigate the bending, buckling, and free vibration behavior of porous beams resting on elastic foundations using HSDT. Hamad et al. (2020) conducted static stability analysis on an FG sandwich beam with a porous core subjected to axial load functions to investigate and optimize critical buckling loads using HSDT. Chami et al. (2022) examined the influence of porosity on fundamental natural frequencies of the simple supported FG sandwich beam with HSDT. Bargozini et al. (2024) studied buckling of a sandwich beam with carbon nano rod reinforced composite and porous core under axially variable forces based on HSDT. Sayyad et al. (2022) investigated the static deformation and free vibration of simply supported porous FG circular beams using the Navier method based on HSDT. Masjedi et al. (2019) investigated the large deflection of FGP beams using a geometrically exact theory with a fully intrinsic formulation and the orthogonal Chebyshev collocation method. Su et al. (2019) investigated the surface effect on the static bending of FGP nanobeams using Reddy's higher-order beam theory. Chinh et al. (2021) applied a point interpolation mesh-free method based on a polynomial basic function to conduct static flexural analysis of an FG sandwich beam with a porous metal core using HSDT. Xin and Kiani (2023) studied the vibration behavior of a thick sandwich beam with an FG porous core resting on an elastic medium using quasi-3D theory and the Navier method.

Among computational methods, FEM has garnered significant attention as one of the prominent numerical techniques for the analysis of FG and sandwich structures over the last few decades (Kahya and Turan 2017; Belarbi et al. 2022; Koutoati et al. 2021a, 2021b; Arslan and Gunes 2018; Van 2022; Vinh et al. 2023; Gupta and Chalak 2023; Vo et al. 2015). Akbaş et.al. (2022) studied the vibration of FG porous, thick beam under the dynamic sine pulse load using FEM. Patil et al. (2023) investigated the static bending and vibration of FG porous sandwich beams with viscoelastic boundary conditions using FSDT and FEM. Zghal et al. (Zghal et al. 2022) explored the effect of porosity on the static bending behavior of FG porous beams using a refined mixed FEM. Malhari Ramteke et al. (2020) introduced an FE solution based on HSDT for the static analysis of FG structures, considering variable grading patterns, including the porosity effect. Vinh et al. (2022) developed a new enhanced finite element model based on the neutral surface position for bending analysis of the FG porous beams with the FSDT. Turan and Adiyaman (2023) used parabolic shear deformation theory to carry out static analysis on two-directional functionally graded (2D-FG) porous beams. Al-Itbi and Noori (2022) investigated the static response of sandwich beams with porous core under uniformly distributed loads along the beam span, using ANSYS finite element software. Grygorowicz et al. (2015) used ANSYS software to analyse the buckling characteristics of sandwich beams with metal foam core. Madenci and Özkılıç (2021) explored the influence of porosity on free vibrational behaviour of FG beam using analytical, ABAQUS FEM package and ANN technique. Using Carrera's Unified Formulation and finite element approximation, Foroutan et al. (2021) investigated post-buckling and large-deflection analysis of a sandwich FG plate with FG porous. Nguyen et al. (2022b) introduced a novel finite element formulation for static bending analysis of functionally graded porous sandwich plates using Quasi-3D theory. Li et al. (2023) conducted nonlinear FE simulations to study nonlinear vibration behavior of FG sandwich beams with auxetic porous Copper core in thermal environments.

Several models have been developed to express the interaction between the beam and elastic foundations. Nguyen Thi (2022) examined the bending, buckling, and free vibration of FG sandwich curved beams resting on the Pasternak foundation using the analytical method and FSDT. Zenkour et al. (2019) used third-order shear deformation theory to carry out the buckling analysis of a size-dependent FG nanobeam resting on a two-parameter elastic foundation. Mohammed et al. (2021) conducted the bending and buckling analysis of the FG

Euler–Bernoulli beam resting on the Winkler-Pasternak elastic foundation. Matinfar et al. (2019) conducted static bending aanalysis of 2D FG porous sandwich beam resting on Winkler-Pasternak Foundation in Hygrothermal environment, Based on the Layerwise Theory and Chebyshev Tau Method. Songsuwan et al. (2018) explored the free vibration and dynamic response of FG sandwich Timoshenko beams resting on an elastic foundation and subjected to a moving harmonic load. Fahsi et al. (2019) proposed a novel refined quasi-3D theory for the free vibration, bending, and buckling analysis of FG porous beams resting on an elastic foundation. Ait Atmane et al. (2017) introduced a novel refined quasi-3D theory for the analysis of free vibration, bending, and buckling of FG porous beams resting on an elastic foundation. Fazzolari (2018) conducted the free vibration and elastic stability analysis of 3D porous FG sandwich beams resting on Winkler-Pasternak elastic foundations using the method of series expansion of displacement components. Ghazwani et al. (2024) performed the high frequency analysis of the FG sandwich nanobeams resting on elastic foundations using nonlocal quasi-3D theory and Navier method.

Based on the above-given literature review, despite many works available on the analysis of single-layer FG porous beams, studies on the analysis of FG sandwich beams with porous core are rare. Shear deformation theories neglecting transverse normal deformations are found to be the most widely used theories for the analysis of FG sandwich beams. Additionally, there is a noticeable absence of studies in the literature addressing the free vibration and buckling analysis of FG sandwich beams with softcore (metal core) using higher order shear and normal deformation theory. Moreover, the application of a quasi-3D theory-based FEM to FG sandwich beams with the porous core is notably restricted due to difficulties in addressing complex problems, such as satisfying the C^1-continuity requirement of the quasi-3D beam theory. The literature on the free vibration and buckling behavior of FG sandwich beams resting on an elastic foundation is limited and fragmented as well. It appears that no study has yet investigated the combined effects of core porosity and elastic foundation on the free vibration and buckling characteristics of FG sandwich beams, considering both shear and normal deformations. In this regard, the present work aims to explore for the first time an investigation into the free vibration and buckling characteristics of FG sandwich beams with porous metal core and sandwich beams with FG porous core resting on a two-parameter Winkler-Pasternak elastic foundation using a new higher-order finite element model based on quasi-3D deformation theory, that account both the effects of transverse shear and normal deformations. The FG material property distribution obeys the power-law rule through the thickness. Three different porosity patterns including uniform, symmetric, and asymmetric are considered. A three-node 15-degrees-of-freedom (DOFs) FE is proposed for the numerical solution. The accuracy and convergence of the proposed model are verified with several numerical examples. A comprehensive parametric investigation is conducted to explore the effects of the skin-to-core thickness ratio, power-law index, boundary conditions, slenderness, porosity coefficient, and porous distribution of the core and elastic foundation parameters on the natural frequencies and critical buckling loads of FG sandwich beams. It is expected that the results of this work evaluate the effect of core porosity and Winkler-Pasternak elastic foundation on the free vibration and buckling behavior of FG sandwich beams with porous core. Additionally, it aims present some benchmark results for the fundamental natural frequencies and buckling loads of FG sandwich beams with porous core.

2 Problem

2.1 Geometrical Configuration

As shown in Fig. 1, a three-layered FG sandwich beam with uniform thickness h, width b, and length L is considered. The top and bottom faces are at $z = \pm h/2$. The beam is supported by a two-parameter elastic foundation with spring constants k_w and k_p, where the former represents the Winkler foundation while the latter is for the Pasternak shear layer. A sandwich beam with FG face layers and an isotropic porous metal core (Type A) and a sandwich beam with isotropic homogenous face layers and an FG porous core (Type B) are examined. The face layers of Type A are graduated from ceramic to metal, whereas the core is porous and entirely metal. The face layers of Type B are made of metal and ceramic layers, respectively, while the core layer is porous and FG from ceramic to metal.

2.2 FG Material Properties

The effective material properties of the FG sandwich beam vary gradually and continuously through the thickness direction according to the power law distribution as

$$\begin{aligned} E(z) &= E_c + \left(E_m - E_c\right)V_c(z) \\ \rho(z) &= \rho_c + \left(\rho_m - \rho_c\right)V_c(z) \end{aligned} \tag{1}$$

for Type A and

$$\begin{aligned} E(z) &= E_m + \left(E_c - E_m\right)V_c(z) \\ \rho(z) &= \rho_m + \left(\rho_c - \rho_m\right)V_c(z) \end{aligned} \tag{2}$$

for Type B. Here, $E(z)$ is Young's modulus, and $\rho(z)$ is the density of the material. Subscripts m and c denote metal and ceramic constituents of material, respectively.

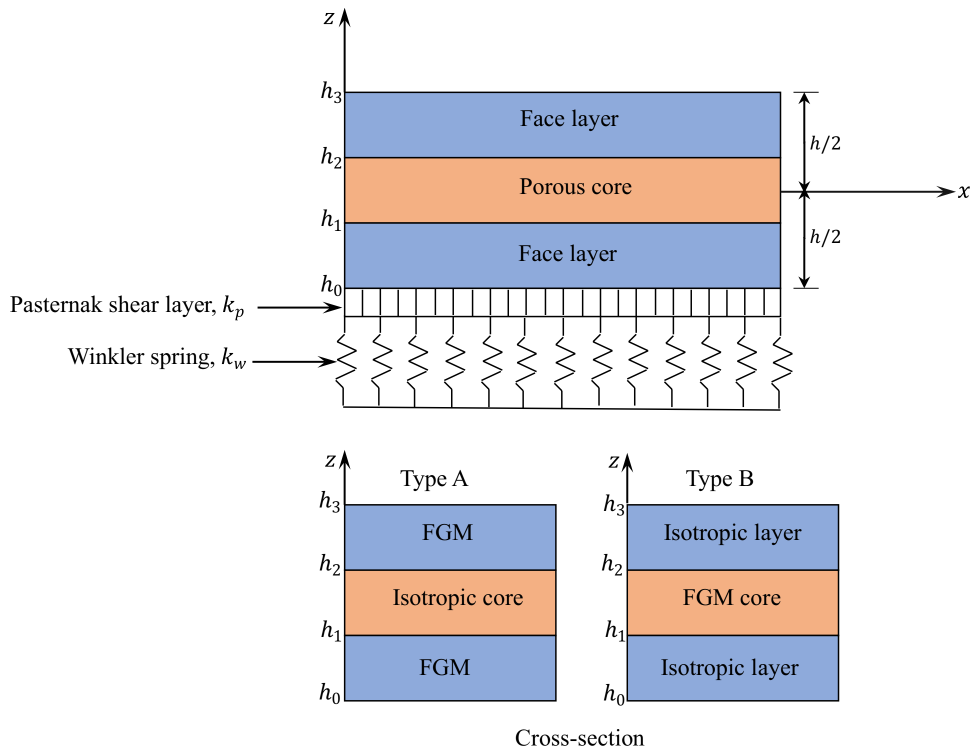

Fig. 1 Configuration of FG sandwich beam resting on elastic foundation

The volume fraction of FG sandwich beams is assumed to obey a power-law function in the direction of thickness which can be stated as follows:

$$
\begin{aligned}
&V_c(z) = \left(\frac{z-h_0}{h_1-h_0}\right)^p \text{ for } z \in [h_0, h_1]\\
&V_c(z) = 1 \text{ for } z \in [h_1, h_2]\\
&V_c(z) = \left(\frac{z-h_3}{h_2-h_3}\right)^p \text{ for } z \in [h_2, h_3]
\end{aligned} \tag{3}
$$

for Type A and

$$
\begin{aligned}
&V_c(z) = 0 \text{ for } z \in [h_0, h_1]\\
&V_c(z) = \left(\frac{z-h_1}{h_2-h_1}\right)^p \text{ for } z \in [h_1, h_2]\\
&V_c(z) = 1 \text{ for } z \in [h_2, h_3]
\end{aligned} \tag{4}
$$

for Type B, where $V_c(z)$ is the volume fraction p is the power-law index.

2.3 Mechanical Properties of Porous Core

Uniform, symmetrical, and asymmetrical distribution of porosity are considered as indicated in Fig. 2. The Young's modulus and the mass density of porous core vary through the thickness according to the following (Chen et al. 2016; Srikarun et al. 2021):

(i) Uniform porosity distribution (UD)

$$
E(z) = E_{\max}[1 - e_0\alpha], \quad \rho(z) = \rho_{\max}\sqrt{1 - e_0\alpha} \text{ for } z \in [h_1, h_2] \tag{5}
$$

(ii) Symmetric porosity distribution (SD)

$$
\begin{aligned}
&E(z) = E_{\max}\left[1 - e_0\cos\left(\frac{\pi z}{h_2 - h_1}\right)\right],\\
&\rho(z) = \rho_{\max}\left[1 - e_m\cos\left(\frac{\pi z}{h_2 - h_1}\right)\right] \text{for} z \in [h_1, h_2]
\end{aligned} \tag{6}
$$

(iii) Asymmetric porosity distribution (ASD)

$$
\begin{aligned}
&E(z) = E_{\max}\left[1 - e_0\cos\left(\frac{\pi z}{2(h_2 - h_1)} + \frac{\pi}{4}\right)\right],\\
&\rho(z) = \rho_{\max}\left[1 - e_m\cos\left(\frac{\pi z}{2(h_2 - h_1)} + \frac{\pi}{4}\right)\right] \text{ for } z \in [h_1, h_2]
\end{aligned} \tag{7}
$$

where $E_{\max}(z)$ and $\rho_{\max}(z)$ are the maximum values of Young's modulus and mass density, e_0 and e_m represent the coefficients of porosity and mass density. Coefficient of α and e_m are obtained as follows:

$$
\alpha = \frac{1}{e_0} - \frac{1}{e_0}\left(\frac{2}{\pi}\sqrt{1 - e_0} - \frac{2}{\pi} + 1\right)^2 e_m = 1 - \sqrt{1 - e_0} \tag{8}
$$

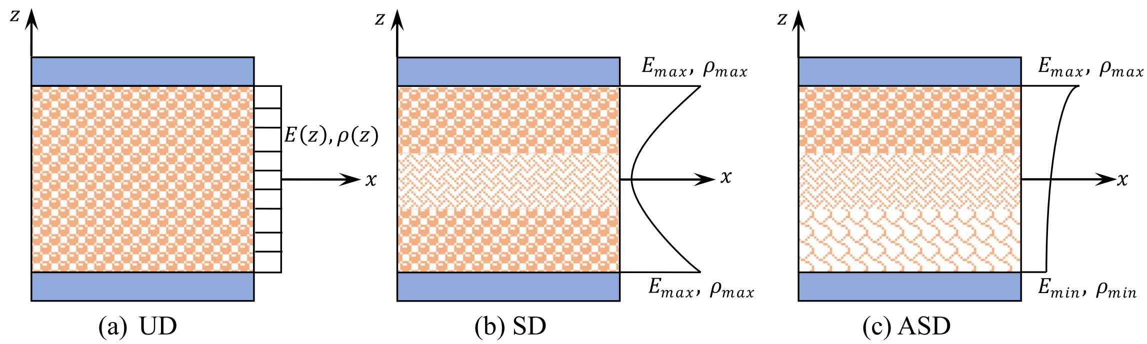

Fig. 2 Porosity distributions in porous core

3 Theoretical Formulation

3.1 Equation of Motion

The displacement field of the present quasi-3D theory is given as follows:

$$\begin{aligned} u(x,z,t) &= u_0(x) - z\frac{\mathrm{d}w_o}{\mathrm{d}x} + f(z)\phi_y(x) \\ w(x,z,t) &= w_0(x) + g(z)\phi_z(x) \end{aligned} \tag{9}$$

where u and w are the displacements of an arbitrary point of FG sandwich beam in x- and z-directions. u_0 and w_0 are displacements at the mid-plane of the beam, ϕ_y and ϕ_z are the shear slope associated with the transverse shear and normal deformations $g(z) = f\prime(z)$, where the shear shape function $f(z)$ is chosen as follows (Reddy 1984):

$$f = z - \frac{4z^3}{3h^2} \tag{10}$$

The strain field of the present theory is obtained by using the strain–displacement relationship from the elasticity theory, and can be expressed as follows:

$$\varepsilon_x = \varepsilon_x^0 - zk_x + f\varepsilon_x^1, \varepsilon_z = g\prime(z)\phi_z(x), \gamma_{xz} = g(z)\gamma_{xz}^0 \tag{11}$$

where

$$\varepsilon_x^0 = \frac{\partial u_0}{\partial x}, k_x = \frac{\partial^2 w_0}{\partial x^2}, \varepsilon_x^1 = \frac{\partial \phi_y}{\partial x}, \gamma_{xz}^0 = \phi_y + \frac{\partial \phi_z}{\partial x} \tag{12}$$

The stress–strain relationship of the FG sandwich beam is given as the following:

$$\begin{Bmatrix} \sigma_x \\ \sigma_z \\ \tau_{xz} \end{Bmatrix} = \begin{bmatrix} Q_{11}(z) & Q_{13}(z) & 0 \\ Q_{13}(z) & Q_{33}(z) & 0 \\ 0 & 0 & Q_{55}(z) \end{bmatrix} \begin{Bmatrix} \varepsilon_x \\ \varepsilon_z \\ \gamma_{xz} \end{Bmatrix} \tag{13}$$

where

$$Q_{11}(z) = Q_{33}(z) = \frac{E(z)}{1-\upsilon^2}, Q_{13}(z) = \frac{\upsilon E(z)}{1-\upsilon^2}, Q_{55}(z) = \frac{E(z)}{2(1+\upsilon)} \tag{14}$$

where υ is Poisson's ratio.

The strain energy of the beam can be expressed as follows:

$$\begin{aligned} U &= \frac{1}{2}\int_0^L \int_{-\frac{h}{2}}^{\frac{h}{2}} \left(\sigma_x\varepsilon_x + \sigma_z\varepsilon_z + \tau_{xz}\gamma_{xz}\right)\mathrm{d}z\mathrm{d}x \\ &= \frac{1}{2}\int_0^L \left[A_{11}\left(\frac{\partial u_0}{\partial x}\right)^2 + E_{11}\left(\frac{\partial^2 w_0}{\partial x^2}\right)^2 + F_{11}\left(\frac{\partial \phi_y}{\partial x}\right)^2 - 2B_{11}\frac{\partial u_0}{\partial x}\frac{\partial^2 w_0}{\partial x^2}\right. \\ &\quad + 2C_{11}\frac{\partial u_0}{\partial x}\frac{\partial \phi_y}{\partial x} - 2D_{11}\frac{\partial^2 w_0}{\partial x^2}\frac{\partial \phi_y}{\partial x} + 2B_{S13}\frac{\partial u_0}{\partial x}\phi_z - 2C_{S13}\frac{\partial^2 w_0}{\partial x^2}\phi_z \\ &\quad \left. + 2E_{S13}\frac{\partial \phi_y}{\partial x}\phi_z + D_{S33}\left(\phi_z\right)^2 + A_{S55}\left(\phi_y\right)^2 + A_{S55}\left(\frac{\partial \phi_z}{\partial x}\right)^2 + 2A_{S55}\frac{\partial \phi_z}{\partial x}\phi_y\right]\mathrm{d}x \end{aligned} \tag{15}$$

where

$$\left[A_{11},B_{11},C_{11},D_{11},E_{11},F_{11},D_{S33}\right]=\int_{-h/2}^{h/2}Q_{11}(z)\left[1,z,f(z),zf(z),z^2,f^2(z),\left[g'(z)\right]^2\right]\mathrm{d}z$$
$$\left[B_{S13},C_{S13},E_{S13}\right]=\int_{-\frac{h}{2}}^{\frac{h}{2}}Q_{13}(z)g'(z)\left[1,z,f(z)\right]\mathrm{d}z \tag{16}$$
$$A_{S55}=\int_{-h/2}^{h/2}Q_{55}(z)\left[g(z)\right]^2\mathrm{d}z$$

The kinetic energy can be defined as

$$\begin{aligned}K&=\frac{1}{2}\int_0^L\int_{-\frac{h}{2}}^{\frac{h}{2}}\rho(z)\left(\dot{U}^2+\dot{W}^2\right)\mathrm{d}z\mathrm{d}x\\&=\frac{1}{2}\int_0^L\left[I_1\left(\frac{\partial u_0}{\partial t}\right)^2+I_3\left(\frac{\partial^2 w_0}{\partial t\partial x}\right)^2+I_6\left(\frac{\partial \phi_y}{\partial t}\right)^2-2I_2\frac{\partial u_0}{\partial t}\frac{\partial^2 w_0}{\partial t\partial x}+2I_4\frac{\partial u_0}{\partial t}\frac{\partial \phi_y}{\partial t}\right.\\&\left.-2I_5\frac{\partial^2 w_0}{\partial t\partial x}\frac{\partial \phi_y}{\partial t}+I_1\left(\frac{\partial w_0}{\partial t}\right)^2+I_8\left(\frac{\partial \phi_z}{\partial t}\right)^2+2I_7\frac{\partial w_0}{\partial t}\frac{\partial \phi_z}{\partial t}\right]\mathrm{d}x\end{aligned} \tag{17}$$

where

$$\left[I_1,I_2,I_3,I_4,I_5,I_6,I_7,I_8\right]=\int_{-h/2}^{h/2}\rho(z)\left[1,z,z^2,f(z),zf(z),f^2(z),g(z),\left[g(z)\right]^2\right]\mathrm{d}z \tag{18}$$

The potential energy due to external axial force can be written as

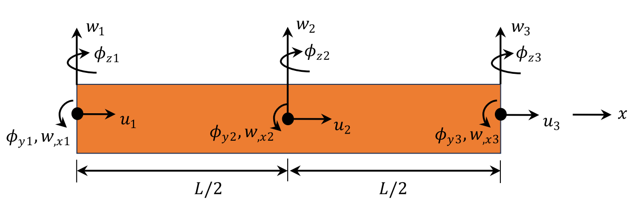

Fig. 3 Three-node higher-order beam element with corresponding DOFs

$$V=-\frac{1}{2}\int_0^L\left[N_0\left(\frac{\partial w_0}{\partial x}\right)^2\right]\mathrm{d}x \tag{19}$$

where N_0 is the axial force.

The strain energy induced by the elastic foundation can be expressed as

$$U_F=\frac{1}{2}\int_0^L\left[\left(k_\mathrm{w}w^2+k_p\left(\frac{\mathrm{d}w}{\partial x}\right)^2\right)\right]\mathrm{d}x \tag{20}$$

where k_w and k_p are the constants of Winkler and shear layer springs.

Total potential energy can then be obtained as follows:

$$\begin{aligned}
\Pi &= U + U_F + V - K \\
&= \frac{1}{2}\int_0^L \left[A_{11}\left(\frac{\partial u_0}{\partial x}\right)^2 + E_{11}\left(\frac{\partial^2 w_0}{\partial x^2}\right)^2 + F_{11}\left(\frac{\partial \phi_y}{\partial x}\right)^2 - 2B_{11}\frac{\partial u_0}{\partial x}\frac{\partial^2 w_0}{\partial x^2} \right. \\
&\quad + 2C_{11}\frac{\partial u_0}{\partial x}\frac{\partial \phi_y}{\partial x} - 2D_{11}\frac{\partial^2 w_0}{\partial x^2}\frac{\partial \phi_y}{\partial x} + 2B_{S13}\frac{\partial u_0}{\partial x}\phi_z - 2C_{S13}\frac{\partial^2 w_0}{\partial x^2}\phi_z \\
&\quad \left. + 2E_{S13}\frac{\partial \phi_y}{\partial x}\phi_z + D_{S33}\left(\phi_z\right)^2 + A_{S55}\left(\phi_y\right)^2 + A_{S55}\left(\frac{\partial \phi_z}{\partial x}\right)^2 + 2A_{S55}\frac{\partial \phi_z}{\partial x}\phi_y \right] \mathrm{d}x \\
&\quad - \frac{1}{2}\int_0^L \left[I_1\left(\frac{\partial u_0}{\partial t}\right)^2 + I_3\left(\frac{\partial^2 w_0}{\partial t \partial x}\right)^2 + I_6\left(\frac{\partial \phi_y}{\partial t}\right)^2 - 2I_2\frac{\partial u_0}{\partial t}\frac{\partial^2 w_0}{\partial t \partial x} + 2I_4\frac{\partial u_0}{\partial t}\frac{\partial \phi_y}{\partial t} \right. \\
&\quad \left. - 2I_5\frac{\partial^2 w_0}{\partial t \partial x}\frac{\partial \phi_y}{\partial t} + I_1\left(\frac{\partial w_0}{\partial t}\right)^2 + I_8\left(\frac{\partial \phi_z}{\partial t}\right)^2 + 2I_7\frac{\partial w_0}{\partial t}\frac{\partial \phi_z}{\partial t} \right] \mathrm{d}x \\
&\quad - \frac{1}{2}\int_0^L \left[N_0\left(\frac{\partial w_0}{\partial x}\right)^2 \right] \mathrm{d}x + \frac{1}{2}\int_0^L \left[\left[\left(k_w\left(w_0 + g\phi_z\right)^2 + k_p\left(\frac{\mathrm{d}\left(w_0 + g\phi_z\right)}{\partial x}\right)^2 \right)\right]\right] \mathrm{d}x
\end{aligned} \tag{21}$$

Lagrange's equation which gives the equation of motion can be written as follows:

$$\frac{\mathrm{d}}{\mathrm{d}t}\left(\frac{\partial \Pi}{\partial \dot{q}_j}\right) - \frac{\partial \Pi}{\partial q_j} = 0 \tag{22}$$

where q_j represents the generalized coordinates, and over dot represents the time derivative.

3.2 Finite Element Formulation

To investigate the free vibration and buckling of FG sandwich beams with porous core resting on an elastic foundation, a three-node higher-order beam finite element having a total of 15 DOFs shown in Fig. 3 is proposed. This new element is formulated based on the present quasi-3D deformation theory. The displacement unknows u_0, ϕ_y and ϕ_z are approximated using a linear polynomial interpolation function $\psi_i(x)$, and w_0 is approximated by a Hermite-cubic polynomial interpolation function $\varphi_i(x)$. The generalized displacements within the element are expressed as:

$$\begin{aligned}
u_0(x,t) &= \sum_{i=1}^{3}\psi_i(x)u_i,\ w_0(x,t) = \sum_{i=1}^{6}\varphi_i(x)w_i \\
\phi_y(x,t) &= \sum_{i=1}^{3}\psi_i(x)\phi_{yi},\ \phi_z(x,t) = \sum_{i=1}^{3}\psi_i(x)\phi_{zi}
\end{aligned} \tag{23}$$

where u_i, w_i, ϕ_{yi}, and ϕ_{zi} are generalized nodal displacement variables and the suffix i donates the corresponding nodal coordinates, $\psi_i(x)$ and $\varphi_i(x)$ are the shape functions which are given in the Appendix.

3.3 Analytical Solution: Ritz Method

Analytical solutions for free vibration and buckling analysis of FG sandwich beams can be obtained using the Ritz method with the present theory. For the Ritz method, the displacement functions $u_0(x)$, $w_0(x)$, $\phi_y(x)$ and $\phi_z(x)$ are presented by the following polynomial series which are satisfy the kinematic boundary conditions,

Table 1 The admissible shape function and kinematics BCs of the beams

BCs	$\psi_j(x)$	$x = 0$	$x = L$
SS	$\frac{x}{l}\left(1-\frac{x}{l}\right)e^{-jx/l}$	$w_0 = 0, \phi_z = 0$	$w_0 = 0, \phi_z = 0$
CC	$\left(\frac{x}{l}\right)^2\left(1-\frac{x}{l}\right)^2 e^{-jx/l}$	$u_0 = 0, w_0 = 0, w_{,x} = 0, \phi_y = 0, \phi_z = 0$	$u_0 = 0, w_0 = 0,$ $w_{,x} = 0, \phi_y = 0$ $,\phi_z = 0$
CF	$\left(\frac{x}{l}\right)^2 e^{-jx/l}$	$u_0 = 0, w_0 = 0, w_{,x} = 0, \phi_y = 0, \phi_z = 0$	–

$$u_0(x,t)=\sum_{j=1}^{m}a_j\psi_{j,x}(x)e^{i\omega t},\quad w_0(x,t)=\sum_{j=1}^{m}b_j\psi_j(x)e^{i\omega t}$$
$$\phi_y(x,t)=\sum_{j=1}^{m}c_j\psi_{j,x}(x)e^{i\omega t},\quad \phi_z(x,t)=\sum_{j=1}^{m}d_j\psi_j(x)e^{i\omega t} \tag{24}$$

where ω is the natural frequency of free vibration of the beam, $\sqrt{i}=1$ the imaginary unit, (a_j,b_j, c_j and d_j) denotes the values to be determine and $\psi_j(x)$ is the admissible shape function. To derive analytical solutions, polynomial and exponential form (Nguyen et al. 2022a) admissible shape functions for various boundary conditions (SS: Simple Supported, CC: Clamped – Clamped, and CF: Clamped – Free beams) are given in the Table 1.

Substituting Eqs. (23) and (24) into Eq. (21), and using the result in Eq. (22) yields the following matrix equations for free vibration and buckling, respectively:

$$[\mathbf{K}-\omega^2\mathbf{M}]\mathbf{\Delta}=0 \tag{25}$$

$$\left[\mathbf{K}-N_0\mathbf{G}\right]\mathbf{\Delta}=0 \tag{26}$$

where $\mathbf{K}$ represents the stiffness matrix, $\mathbf{M}$ is the mass matrix, $\mathbf{G}$ is the geometric stiffness matrix, and $\mathbf{\Delta}$ is the vector of unknown coefficients. ω and N_0 are the natural frequency and buckling load, respectively. The components of these matrices are given in the Appendix.

4 Numerical Results and Discussion

This section presents various numerical examples to validate the accuracy of the proposed FE model. FG layers of sandwich beams are assumed to be made from a mixture of Alumina (Al_2O_3) and Aluminum (Al). A parametric study is performed to evaluate the effects of the power-law index, span-to-height ratio, skin–core-skin thickness ratio, boundary conditions, elastic foundation parameters, and porosity on the free vibration and buckling behavior of FG sandwich beams. The material properties adopted here are: $E_c=380\text{GPa}$, $\rho_c=3960\text{kg/m}^3$, $\nu_c=0.3$ for ceramic material (Alumina) and $E_m=70\text{GPa}$, $\rho_m=2702\text{kg/m}^3$, $\nu_m=0.3$ for metal material (Aluminum). Table 1 shows the kinematic relations for various boundary conditions. As seen, three different boundary conditions namely simple-simple (SS), clamped–clamped (CC), and clamped-free (CF) are considered. For simplicity, the natural frequency, critical buckling load, and elastic foundation parameters are, respectively, defined in the following nondimensional forms:

$$\overline{\omega}=\frac{\omega L^2}{h}\sqrt{\frac{\rho_m}{E_m}},\overline{N}_{cr}=\frac{12N_{cr}L^2}{E_mh^3},K_w=\frac{12k_wL^4}{E_mh^3},K_p=\frac{12k_pL^2}{E_mh^3} \tag{27}$$

Table 2 Convergence study of nondimensional fundamental natural frequencies of the beams with various boundary conditions and length-to-thickness ratios

Beam	Number of elements	$L/h=5$			$L/h=20$		
		SS	CC	CF	SS	CC	CF
Type A	4	2.6819	5.3848	0.9942	2.8375	6.4359	2.4778
	8	2.6819	5.3232	0.9915	2.8375	6.3986	2.4716
	12	2.6819	5.3038	0.9907	2.8375	6.3870	2.4697
	16	2.6819	5.2954	0.9903	2.8375	6.3814	2.4688
	20	2.6819	5.2914	0.9901	2.8375	6.3781	2.4683
	24	2.6819	5.2894	0.9900	2.8375	6.3759	2.4680
	28	2.6819	5.2883	0.9900	2.8375	6.3744	2.4677
	32	2.6819	5.2877	0.9899	2.8375	6.3733	2.4676
	Ritz solution	2.6819	5.2929	0.9901	2.8375	6.3901	1.0147
	HSDT (Vo et al. 2014)	2.6773	5.2311	0.9847	2.8371	6.3509	1.0130
Type B	4	4.0997	8.5814	1.5059	4.2714	9.7152	1.5316
	8	4.0996	8.5015	1.5025	4.2713	9.6665	1.5283
	12	4.0996	8.4749	1.5013	4.2713	9.6519	1.5272
	16	4.0996	8.4626	1.5007	4.2713	9.6447	1.5267
	20	4.0996	8.4566	1.5004	4.2713	9.6404	1.5265
	24	4.0996	8.4535	1.5002	4.2713	9.6376	1.5263
	28	4.0996	8.4519	1.5002	4.2713	9.6356	1.5262
	32	4.0996	8.4510	1.5001	4.2713	9.6341	1.5261
	Ritz solution	4.0996	8.4521	1.4967	4.2713	9.6537	1.5247
	HSDT (Nguyen et al. 2015)	4.0691	8.3282	1.4840	4.2445	9.5451	1.5145
	Quasi-3D (Nguyen et al. 2016)	4.0996	8.4529	1.5001	4.2711	9.6404	1.5264

Table 3 Convergence study of nondimensional critical buckling loads of the beams with various boundary conditions and length-to-thickness ratios

Beam	Number of elements	$L/h = 5$			$L/h = 20$		
		SS	CC	CF	SS	CC	CF
Type A	4	9.1351	29.5573	2.4298	9.8211	39.1240	2.4778
	8	9.1351	29.5358	2.4211	9.8211	38.9236	2.4716
	12	9.1351	29.5296	2.4177	9.8211	38.8679	2.4697
	16	9.1351	29.5264	2.4164	9.8211	38.8422	2.4688
	20	9.1351	29.5246	2.4158	9.8211	38.8277	2.4683
	24	9.1351	29.5237	2.4156	9.8211	38.8186	2.4680
	28	9.1351	29.5233	2.4154	9.8211	38.8124	2.4677
	32	9.1351	29.5230	2.4153	9.8211	38.8081	2.4676
	Ritz solution	9.1351	29.5271	2.4157	9.8211	38.9343	2.4681
	HSDT (Vo et al. 2014)	8.9519	28.0272	2.4057	9.8067	38.4910	2.4635
Type B	4	28.7899	100.7534	7.4741	30.0196	120.3349	7.5569
	8	28.7882	100.6137	7.4503	30.0195	119.6885	7.5406
	12	28.7881	100.5869	7.4410	30.0195	119.5359	7.5356
	16	28.7881	100.5730	7.4375	30.0195	119.4671	7.5333
	20	28.7881	100.5653	7.4359	30.0195	119.4281	7.5319
	24	28.7881	100.5614	7.4351	30.0195	119.4032	7.5311
	28	28.7881	100.5594	7.4346	30.0195	119.3860	7.5304
	32	28.7881	100.5583	7.4343	30.0195	119.3736	7.5300
	Ritz solution	28.7881	100.5588	7.4236	30.0195	119.6879	7.5279
	HSDT (Nguyen et al. 2015)	27.9314	94.6117	7.3149	29.6120	117.0384	7.4254
	Quasi-3D (Nguyen et al. 2016)	28.7884	100.5883	7.4344	30.0168	119.4172	7.5312

Table 4 Comparison of nondimensional fundamental natural frequencies of FG sandwich beams (Type A)

L/h	BC	Theory	p					
			0	0.5	1	2	5	10
5	SS	FEM	2.6819	3.9979	4.3730	4.6536	4.8650	4.9416
		Ritz method	2.6819	3.9979	4.3730	4.6536	4.8650	4.9416
		HSDT (Vo et al. 2014)	2.6773	4.0504	4.4270	4.7047	4.9038	4.9700
	CC	FEM	5.2894	7.1181	7.5838	7.9629	8.3204	8.4894
		Ritz method	5.2929	7.1243	7.5909	7.9706	8.3285	8.4976
		HSDT (Vo et al. 2014)	5.2311	7.2456	7.8056	8.2835	8.7255	8.9195
	CF	FEM	0.9900	1.5095	1.6620	1.7747	1.8556	1.8825
		Ritz method	0.9901	1.5095	1.6620	1.7748	1.8556	1.8826
		HSDT (Vo et al. 2014)	0.9847	1.5211	1.6691	1.7745	1.8444	1.8652
20	SS	FEM	2.8375	4.4165	4.8944	5.2452	5.4851	5.5583
		Ritz method	2.8375	4.4165	4.8944	5.2452	5.4851	5.5583
		HSDT (Vo et al. 2014)	2.8371	4.4160	4.8938	5.2445	5.4843	5.5575
	CC	FEM	6.3759	9.7936	10.8088	11.5576	12.0853	12.2560
		Ritz method	6.3901	9.8189	10.8371	11.5881	12.1170	12.2880
		HSDT (Vo et al. 2014)	6.3509	9.7587	10.7706	11.5168	12.0423	12.2122
	CF	Present	1.0146	1.5818	1.7540	1.8803	1.9663	1.9924
		FEM	1.0147	1.5819	1.7541	1.8804	1.9664	1.9925
		Ritz method	1.0130	1.5796	1.7516	1.8778	1.9636	1.9896

Table 5 Comparison of nondimensional fundamental natural frequencies of FG sandwich beams (Type B)

L/h	BC	Theory	p					
			0	0.5	1	2	5	10
5	SS	FEM	4.0996	3.8439	3.7165	3.6112	3.5512	3.5417
		Ritz method	4.0996	3.8439	3.7165	3.6112	3.5512	3.5417
		HSDT (Nguyen et al. 2015)	4.0691	3.7976	3.6636	3.553	3.4914	3.483
		Quasi-3D (Nguyen et al. 2016)	4.0996	3.8438	3.7172	3.6119	3.5513	3.5413
	CC	FEM	8.4535	7.8938	7.5898	7.2904	7.0069	6.8815
		Ritz method	8.4525	7.8932	7.5894	7.2903	7.0071	6.8818
		HSDT (Nguyen et al. 2015)	8.3282	7.7553	7.4487	7.1485	6.8702	6.7543
		Quasi-3D (Nguyen et al. 2016)	8.4529	7.8924	7.5904	7.2898	7.0032	6.8757
	CF	FEM	1.5002	1.4078	1.3626	1.3271	1.3112	1.3119
		Ritz method	1.5003	1.4078	1.3626	1.3271	1.3112	1.3119
		HSDT (Nguyen et al. 2015)	1.4840	1.3865	1.3393	1.3022	1.2857	1.2867
		Quasi-3D (Nguyen et al. 2016)	1.5001	1.4076	1.3627	1.3273	1.3113	1.3118
20	SS	FEM	4.2713	4.0146	3.8916	3.7995	3.7702	3.7826
		Ritz method	4.2713	4.0146	3.8916	3.7995	3.7702	3.7826
		HSDT (Nguyen et al. 2015)	4.2445	3.9695	3.8387	3.7402	3.7081	3.7214
		Quasi-3D (Nguyen et al. 2016)	4.2711	4.0143	3.8923	3.8003	3.7708	3.7831
	CC	FEM	9.6376	9.0508	8.7668	8.5477	8.4604	8.4738
		Ritz method	9.6546	9.0658	8.7809	8.5613	8.4741	8.488
		HSDT (Nguyen et al. 2015)	9.5451	8.9243	8.6264	8.3959	8.3047	8.3205
		Quasi-3D (Nguyen et al. 2016)	9.6404	9.0524	8.7701	8.5509	8.4627	8.4755
	CF	FEM	1.5263	1.4344	1.3904	1.3576	1.3475	1.3523
		Ritz method	1.5264	1.4344	1.3905	1.3577	1.3476	1.3523
		HSDT (Nguyen et al. 2015)	1.5145	1.4165	1.37	1.335	1.3241	1.3292
		Quasi-3D (Nguyen et al. 2016)	1.5264	1.4344	1.3907	1.358	1.3478	1.3525

Table 6 Comparison of nondimensional critical buckling loads of FG sandwich beams (Type A)

L/h	BC	Theory	p					
			0	0.5	1	2	5	10
5	SS	FEM	9.1351	21.7614	26.9366	31.5445	35.6386	37.3250
		Ritz method	9.1351	21.7614	26.9366	31.5445	35.6386	37.3250
		HSDT (Vo et al. 2014)	9.8067	25.6086	32.5803	38.7192	43.7637	45.6040
	CC	FEM	29.5237	58.3337	68.8601	78.7220	88.8611	93.8148
		Ritz method	29.5271	58.3461	68.8748	78.7385	88.8791	93.8336
		HSDT (Vo et al. 2014)	28.0272	56.1398	66.4523	76.0626	85.8462	90.5815
	CF	FEM	2.4156	6.1749	7.8042	9.2408	10.4430	10.8956
		Ritz method	2.4157	6.1752	7.8047	9.2413	10.4436	10.8962
		HSDT (Vo et al. 2014)	2.4057	6.1578	7.7858	9.2209	10.4208	10.8716
20	SS	FEM	9.8211	25.6411	32.6255	38.7731	43.8252	45.6685
		Ritz method	9.8211	25.6411	32.6255	38.7731	43.8252	45.6685
		HSDT (Vo et al. 2014)	9.8067	25.6086	32.5803	38.7192	43.7637	45.6040
	CC	FEM	38.8186	99.2672	125.4954	148.6238	167.9729	175.2486
		Ritz method	38.9343	99.6031	125.9248	149.1336	168.5475	175.8463
		HSDT (Vo et al. 2014)	38.4910	98.5240	24.5720	47.5350	66.7330	73.9460
	CF	FEM	2.4680	6.4753	8.2526	9.8164	11.0958	11.5589
		Ritz method	2.4681	6.4757	8.2531	9.8170	11.0965	11.5596
		HSDT (Vo et al. 2014)	2.4635	6.4654	8.2402	9.8018	11.0792	6.4654

Table 7 Comparison of nondimensional critical buckling loads of FG sandwich beams (Type B)

L/h	BC	Theory	p					
			0	0.5	1	2	5	10
5	SS	FEM	28.7881	23.8572	21.6294	19.7893	18.5216	18.1383
		Ritz method	28.7881	23.8572	21.6294	19.7893	18.5216	18.1383
		HSDT (Nguyen et al. 2015)	27.9314	22.9869	20.7762	18.9588	17.732	17.3775
		Quasi-3D (Nguyen et al. 2016)	28.7884	23.8554	21.6374	19.7957	18.5212	18.1329
	CC	FEM	100.5614	82.4740	73.9071	66.1303	59.3190	56.4930
		Ritz method	100.5629	82.477	73.9112	66.1354	59.3243	56.4987
		HSDT (Nguyen et al. 2015)	94.6117	77.5129	69.4877	62.2249	55.9446	53.3734
		Quasi-3D (Nguyen et al. 2016)	100.5883	82.4783	73.9348	66.1308	59.2628	56.4049
	CF	FEM	7.4351	6.1847	5.6286	5.1864	4.9216	4.8653
		Ritz method	7.4354	6.1849	5.6288	5.1866	4.9218	4.8655
		HSDT (Nguyen et al. 2015)	7.3149	6.0286	5.4629	5.0154	4.7534	4.7024
		Quasi-3D (Nguyen et al. 2016)	7.4344	6.1836	5.6304	5.1884	4.9228	4.8658
20	SS	FEM	30.0195	24.9952	22.772	21.0254	20.0317	19.8573
		Ritz method	30.0195	24.9952	22.772	21.0254	20.0317	19.8573
		HSDT (Nguyen et al. 2015)	29.612	24.414	22.1386	20.3581	19.3639	19.2058
		Quasi-3D (Nguyen et al. 2016)	30.0168	24.9914	22.7796	21.0343	20.0386	19.8622
	CC	FEM	119.4032	99.2755	90.3305	83.2242	78.9796	78.0853
		Ritz method	119.7827	99.5671	90.5848	83.4516	79.1967	78.3045
		HSDT (Nguyen et al. 2015)	117.0384	96.4573	87.4069	80.2465	76.0539	75.2379
		Quasi-3D (Nguyen et al. 2016)	119.4172	99.2742	90.3696	83.2627	79.0045	78.0989
	CF	FEM	7.5311	6.2708	5.7138	5.2775	5.0325	4.9920
		Ritz method	7.5315	6.2711	5.7140	5.2778	5.0327	4.9922
		HSDT (Nguyen et al. 2015)	7.4254	6.1225	5.5529	5.1084	4.8634	4.8269
		Quasi-3D (Nguyen et al. 2016)	7.5312	6.2702	5.716	5.28	5.0345	4.9934

4.1 Convergency and Validation

To demonstrate the accuracy of the present quasi-3D theory and the proposed FE model, free vibration and buckling analyses of FG sandwich beams without the elastic foundation and porosity are performed. To the best of the authors' knowledge, natural frequencies, and critical buckling loads of FG sandwich beams with porous metal core and sandwich beams with FG porous core resting on a Winkler-Pasternak foundation, have not been documented in available literature.

Tables 2 and 3 show the convergency of the proposed FE for simple-simple (SS), clamped–clamped (CC), and clamped-free (CF) beams with length-to-thickness ratios of $L/h = 5$ and 20. As seen, the proposed FE yields highly accurate results, showing excellent agreement with those of previous studies as well as that of Ritz method. It is noticed that the nondimensional fundamental natural frequencies and critical buckling loads of simply supported (SS) beams converge rapidly with four elements for both beam types. Conversely, in the case of clamped–clamped (CC) and clamped-free (CF) boundary conditions, consistent outcomes are achieved after twenty elements. To ensure accuracy, 24 beam elements are, therefore, used for further analyses.

Tables 4, 5, 6, 7 show a comparison of the nondimensional fundamental natural frequencies and critical buckling loads of FG sandwich beams. Length-to-thickness ratios of $L/h = 5$ and 20, skin–core-skin thickness ratios of 1–2–1, and three boundary conditions are considered. The results are compared to those of the references, which are based on HSDT (Vo et al. 2014; Nguyen et al. 2015) and Quasi-3D theory (Nguyen et al. 2016) as well as the Ritz solution obtained with the present theory by the authors. The study, based on quasi-3D theory (Nguyen et al. 2016) investigated only the free vibration and buckling characteristics of sandwich beams with FG core (Type B). Fundamental natural frequencies and critical buckling loads of FG sandwich beams with metal core (Type A) obtained with a quasi-3D theory are not available in the literature. Therefore, the results of Type A are only compared to HSDT (Vo et al. 2014) and the Ritz solution in order to validate the accuracy of the results and present some benchmark results for the fundamental natural frequencies and buckling loads of FG sandwich beams with softcore. It is observed that the solutions derived from the proposed FE model are in excellent agreement with the studies that consider transverse normal deformations. The slight difference with the current reference studies using HSDT is

Table 8 The first three nondimensional natural frequencies of FG sandwich beams (Type A)

Mode	BC	Theory	p					
			0	0.5	1	2	5	10
1	SS	FEM	2.6819	3.9979	4.3730	4.6536	4.8650	4.9416
		Ritz method	2.6819	3.9979	4.3730	4.6536	4.8650	4.9416
		HSDT (Vo et al. 2014)	2.6773	4.0504	4.4270	4.7047	4.9038	4.9700
	CC	FEM	5.2894	7.1181	7.5838	7.9629	8.3204	8.4894
		Ritz method	5.2929	7.1243	7.5909	7.9706	8.3285	8.4976
		HSDT (Vo et al. 2014)	5.2311	7.2456	7.8056	8.2835	8.7255	8.9195
	CF	FEM	0.9900	1.5095	1.6620	1.7747	1.8556	1.8825
		Ritz method	0.9901	1.5095	1.6620	1.7748	1.8556	1.8826
		HSDT (Vo et al. 2014)	0.9847	1.5211	1.6691	1.7745	1.8444	1.8652
2	SS	FEM	9.3379	12.8786	13.7986	14.5280	15.1801	15.4727
		Ritz method	9.3379	12.8786	13.7986	14.5280	15.1801	15.4727
		HSDT (Vo et al. 2014)	9.2909	12.8310	13.7464	14.4701	15.1156	15.4047
	CC	FEM	12.1812	15.4688	16.2925	17.0136	17.7724	18.1649
		Ritz method	12.5970	16.5814	17.6667	18.6710	19.0927	19.5200
		HSDT (Vo et al. 2014)	12.5225	16.0881	16.9638	17.7202	18.5077	18.9119
	CF	FEM	5.3586	7.4934	8.0584	8.5002	8.8818	9.0470
		Ritz method	5.3591	7.4940	8.0590	8.5009	8.8826	9.0477
		HSDT (Vo et al. 2014)	5.3234	7.4544	8.0182	8.4585	8.8373	9.0006
3	SS	FEM	17.9179	23.2515	24.5620	25.6794	26.8221	27.4001
		Ritz method	17.9178	23.2514	24.5619	25.6792	26.8219	27.3999
		HSDT (Vo et al. 2014)	17.7751	23.1294	24.4327	25.5391	26.6663	27.2351
	CC	FEM	16.4664	20.9126	22.6223	24.1082	25.4190	25.9665
		Ritz method	16.4673	20.9137	22.6235	24.1094	25.4203	25.9678
		HSDT (Vo et al. 2014)	15.7120	19.9545	21.5859	23.0036	24.2544	24.7768
	CF	FEM	8.2332	10.4563	11.3112	12.0541	12.7095	12.9832
		Ritz method	8.2332	10.4563	11.3112	12.0541	12.7095	12.9832
		HSDT (Vo et al. 2014)	7.8545	9.9753	10.7909	11.4996	12.1248	12.3860

since they neglected the effect of the transverse normal strain. Furthermore, the tables illustrate that as the power-law index increases, the fundamental natural frequencies and critical buckling loads increase in FG sandwich beams with porous metal core, whereas they decrease for sandwich beams with FG porous core. This is explained by the fact that a higher value of p indicates a higher proportion of the ceramic phase, leading to an increase in Young's modulus and consequently in the bending stiffness. The observed correlation between the power-law index and the beam's responses underlines the significance of material composition in determining the overall free vibration and buckling responses of FG sandwich beams. Consequently, the choice of the power-law index is crucial for predicting and adopting the mechanical performance of the FG sandwich beams for specific applications.

For the sake of completeness, the first three natural frequencies of 1–2–1 FG sandwich beams are presented for $L/h = 5$ in Tables 8 and 9. Noticeably, accounting for normal strain effects yields higher outcomes, emphasizing the significance of considering such an effect.

4.2 Effect of Porosity

In Tables 10 and 11, the nondimensional fundamental natural frequencies are computed for the FG sandwich beam with configuration 1–2–1 considering three core porosity patterns with different values of porosity coefficient ($e_0 = 0.4, 0.6, 0.8$) under three different foundation conditions: no elastic foundation, a Winkler foundation, and a Pasternak foundation. The power-law index is set to $p = 2$, and length-to-thickness ratios $L/h = 5$ and 20 are considered. The results indicate a consistent trend across all boundary conditions in both types. For all three types of porosity patterns and length-to-thickness ratios, the nondimensional fundamental natural frequencies increase with the porosity coefficient. This is because increasing the porosity reduces both the bending stiffness and the mass density of the beam. The combination of these two effects increases the natural frequency of the beam overall. However, a notable exception is observed for CC beams when $L/h = 5$, where the nondimensional fundamental natural frequencies decrease as the porosity coefficient increases. This phenomenon can be

Table 9 The first three nondimensional natural frequencies of FG sandwich beams (Type B)

Mode	BC	Theory	p					
			0	0.5	1	2	5	10
1	SS	FEM	4.0996	3.8439	3.7165	3.6112	3.5512	3.5417
		Ritz method	4.0996	3.8439	3.7165	3.6112	3.5512	3.5417
		HSDT (Nguyen et al. 2015)	4.0691	3.7976	3.6636	3.5530	3.4914	3.4830
	CC	FEM	8.4535	7.8938	7.5898	7.2904	7.0069	6.8815
		Ritz method	8.4525	7.8932	7.5894	7.2903	7.0071	6.8818
		HSDT (Nguyen et al. 2015)	8.3282	7.7553	7.4487	7.1485	6.8702	6.7543
	CF	FEM	1.5002	1.4078	1.3626	1.3271	1.3112	1.3119
		Ritz method	1.5003	1.4078	1.3626	1.3271	1.3112	1.3119
		HSDT (Nguyen et al. 2015)	1.4840	1.3865	1.3393	1.3022	1.2857	1.2867
2	SS	FEM	14.7402	13.7534	13.2273	12.7289	12.2980	12.1255
		Ritz method	14.7403	13.7536	13.2275	12.7291	12.2982	12.1257
		HSDT (Nguyen et al. 2015)	14.5921	13.5629	13.0215	12.5117	12.0822	11.9168
	CC	FEM	20.1544	18.7387	17.9222	17.0450	16.0975	15.6427
		Ritz method	20.7864	19.3438	18.5249	17.6623	16.7505	16.3147
		HSDT (Nguyen et al. 2015)	19.8886	18.4463	17.6290	16.7552	15.8266	15.3878
	CF	FEM	8.4115	7.8472	7.5479	7.2682	7.0355	6.9473
		Ritz method	8.4122	7.8478	7.5484	7.2686	7.0359	6.9477
		HSDT (Nguyen et al. 2015)	8.3149	7.7255	7.4173	7.1308	6.8984	6.8139
3	SS	FEM	29.1374	27.0784	25.9265	24.7440	23.4231	22.7558
		Ritz method	29.1329	27.0748	25.9235	24.7414	23.4232	22.7559
		HSDT (Nguyen et al. 2015)	28.7653	26.6542	25.4901	24.3022	23.1254	22.5934
	CC	FEM	34.4183	31.9232	30.4419	28.7950	26.9517	26.0580
		Ritz method	34.5185	32.0116	30.5248	28.8733	27.0258	26.1303
		HSDT (Nguyen et al. 2015)	34.0624	31.5260	30.0458	28.4068	26.5927	25.7241
	CF	FEM	14.6578	13.6956	13.1485	12.5521	11.8995	11.5818
		Ritz method	14.6579	13.6956	13.1486	12.5521	11.8995	11.5818
		HSDT (Nguyen et al. 2015)	14.0712	13.2130	12.7196	12.1683	11.5477	11.2377

explained by the fact that when the length-to-thickness ratio is relatively small $L/h = 5$, the reduction in bending stiffness becomes more significant than the reduction in mass density for CC beams. As a result, the natural frequency of the beam decreases overall. The nondimensional fundamental natural frequencies of sandwich beams are arranged in descending order of porosity as follows: symmetrical, asymmetrical, and uniform patterns. It is evident that the nondimensional fundamental natural frequencies of FG sandwich porous beams of Type A (with FG face layers and an isotropic porous metal core) are significantly higher than those of Type B (with isotropic homogeneous face layers and an FG porous core) for all boundary conditions, porosity distributions, and elastic foundation cases considered. This can be attributed to the presence of FG face layers, which provide superior bending stiffness compared to the isotropic homogeneous face layers in Type B beams, outweighing the effect of porosity on the mass density of the beam.

Similarly, Tables 12 and 13 show the variation of the nondimensional critical buckling load of the beams for the core porosity coefficient of three different porosity patterns and the L/h ratio for various BCs. Regardless of the porosity patterns or and L/h ratio, the nondimensional critical buckling loads decrease as the parameter e_0 increases. This behavior is attributed to an increase in core porosity that reduces the beam's bending stiffness, resulting in a reduction in critical buckling loads. It is noticed that for all conditions, the presence of elastic foundation yields an increment in nondimensional fundamental natural frequencies and critical buckling loads of FG sandwich beams. The inclusion of a shear layer further enhances this effect by increasing the shear stiffness of the beams.

Figures 4 and 5 visualize the variation of nondimensional fundamental natural frequencies and critical buckling loads of the SS beams with respect to porosity coefficients for three different cases: Case 1 with $K_w = 0$ and $K_p = 0$, Case 2 with $K_w = 10$ and $K_p = 0$, and Case 3 with $K_w = 10$ and $K_p = 10$. The skin–core-skin thickness ratio of 1–2–1, $L/h = 10$, $p = 5$, and symmetric porosity distribution are considered. It is revealed that for all cases, nondimensional fundamental natural frequencies increase as the porosity coefficient increases. In terms of critical buckling loads,

Table 10 Variation of nondimensional fundamental natural frequencies of Type A beam under different BCs, porosity distribution, and elastic foundation (1–2–1, $p = 2$)

L/h	K_w	K_p	BCs	e_0								
				UD			SD			ASD		
				0.4	0.6	0.8	0.4	0.6	0.8	0.4	0.6	0.8
5	0	0	SS	4.7059	4.7404	4.7894	4.7090	4.7507	4.8199	4.7102	4.7541	4.8272
			CC	7.8424	7.7661	7.6740	7.8350	7.7761	7.7466	7.8554	7.8114	7.8015
			CF	1.8082	1.8310	1.8632	1.8105	1.8358	1.8736	1.8095	1.8347	1.8727
	100	0	SS	5.4475	5.5077	5.5929	5.4503	5.5165	5.6188	5.4512	5.5193	5.6249
			CC	8.3153	8.2639	8.2071	8.3083	8.2733	8.2750	8.3275	8.3064	8.3263
			CF	3.2941	3.3561	3.4434	3.2953	3.3586	3.4487	3.2948	3.3580	3.4482
	100	10	SS	6.0915	6.1720	6.2860	6.0940	6.1799	6.3088	6.0948	6.1823	6.3141
			CC	8.7913	8.7618	8.7362	8.7847	8.7709	8.8006	8.8029	8.8021	8.8488
			CF	3.7149	3.7825	3.8776	3.7156	3.7846	3.8833	3.7157	3.7849	3.8843
20	0	0	SS	5.3859	5.4838	5.6234	5.3957	5.5004	5.6503	5.3888	5.4897	5.6358
			CC	11.8095	11.9823	12.2269	11.8267	12.0153	12.2924	11.8174	12.0025	12.2775
			CF	1.9321	1.9682	2.0198	1.9357	1.9742	2.0292	1.9331	1.9701	2.0236
	100	0	SS	6.0566	6.1709	6.3335	6.0653	6.1856	6.3573	6.0591	6.1762	6.3444
			CC	12.1301	12.3119	12.5693	12.1468	12.3441	12.6329	12.1377	12.3315	12.6185
			CF	3.3787	3.4483	3.5467	3.3808	3.4517	3.5521	3.3793	3.4494	3.5489
	100	10	SS	6.6526	6.7812	6.9636	6.6605	6.7946	6.9853	6.6549	6.7860	6.9736
			CC	12.5032	12.6945	12.9651	12.5194	12.7257	13.0270	12.5107	12.7138	13.0134
			CF	3.8409	3.9203	4.0323	3.8428	3.9234	4.0374	3.8415	3.9214	4.0346

Table 11 Variation of nondimensional fundamental natural frequencies of Type B beam under different BCs, porosity distribution, and elastic foundation (1–2–1, $p = 2$)

L/h	K_w	K_p	BCs	e_0								
				UD			SD			ASD		
				0.4	0.6	0.8	0.4	0.6	0.8	0.4	0.6	0.8
5	0	0	SS	3.6131	3.6166	3.6252	3.6202	3.6343	3.6699	3.5868	3.5827	3.5982
			CC	7.1820	7.1076	7.0061	7.1953	7.1516	7.1346	7.1899	7.1531	7.1535
			CF	1.3321	1.3366	1.3447	1.3348	1.3429	1.3598	1.3201	1.3197	1.3267
	100	0	SS	4.5056	4.5472	4.6100	4.5102	4.5594	4.6422	4.4810	4.5140	4.5784
			CC	7.6746	7.6291	7.5701	7.6865	7.6690	7.6872	7.6795	7.6670	7.6990
			CF	3.0227	3.0831	3.1700	3.0224	3.0833	3.1722	3.0123	3.0669	3.1477
	100	10	SS	5.2393	5.3077	5.4086	5.2423	5.3167	5.4334	5.2151	5.2740	5.3729
			CC	8.1946	8.1745	8.1523	8.2052	8.2111	8.2608	8.1987	8.2090	8.2710
			CF	3.4809	3.5507	3.6504	3.4803	3.5507	3.6531	3.4709	3.5355	3.6303
20	0	0	SS	3.8259	3.8479	3.8853	3.8341	3.8659	3.9254	3.7865	3.7894	3.8139
			CC	8.5922	8.6305	8.6968	8.6102	8.6716	8.7920	8.5107	8.5127	8.5630
			CF	1.3673	1.3754	1.3891	1.3702	1.3818	1.4033	1.3530	1.3541	1.3629
	100	0	SS	4.7030	4.7598	4.8460	4.7088	4.7729	4.8756	4.6676	4.7065	4.7787
			CC	9.0168	9.0736	9.1661	9.0335	9.1119	9.2551	8.9374	8.9585	9.0339
			CF	3.0594	3.1228	3.2139	3.0594	3.1233	3.2162	3.0478	3.1042	3.1873
	100	10	SS	5.4315	5.5139	5.6357	5.4358	5.5238	5.6591	5.3980	5.4628	5.5694
			CC	9.5085	9.5852	9.7057	9.5238	9.6206	9.7885	9.4314	9.4733	9.5759
			CF	3.5342	3.6090	3.7164	3.5339	3.6090	3.7180	3.5217	3.5889	3.6872

Table 12 Variation of nondimensional critical buckling loads of Type A beam under different BCs, porosity distribution, and elastic foundation (1–2–1, $p = 2$)

L/h	K_w	K_p	BCs	e_0								
				UD			SD			ASD		
				0.4	0.6	0.8	0.4	0.6	0.4	0.4	0.6	0.8
5	0	0	SS	30.2135	29.3521	28.2242	30.2522	29.4800	28.5960	30.2713	29.5285	28.6935
			CC	71.8155	67.5924	62.3648	71.6677	67.7367	63.4885	72.0437	68.3602	64.4079
			CF	9.0669	8.9569	8.8143	9.0947	9.0077	8.9074	9.0784	8.9851	8.8807
	100	0	SS	40.4787	39.6141	38.4818	40.5171	39.7417	38.8541	40.5367	39.7910	38.9527
			CC	79.2025	74.9231	69.6113	79.0513	75.0673	70.7524	79.4333	75.7014	71.6890
			CF	21.5344	21.1865	20.7169	21.5585	21.2521	20.8918	21.5590	21.2607	20.9172
	100	10	SS	50.6047	49.7369	48.6002	50.6428	49.8643	48.9730	50.6628	49.9143	49.0728
			CC	89.3498	85.0605	79.7355	89.1976	85.2041	80.8784	89.5810	85.8405	81.8182
			CF	30.9754	30.6127	30.1244	31.0047	30.6879	30.3162	31.0018	30.6912	30.3341
20	0	0	SS	38.3449	38.0925	37.7847	38.4845	38.3238	38.1473	38.3856	38.1756	37.9511
			CC	145.8516	144.0979	141.8237	146.2983	144.9112	143.3127	146.0365	144.5486	142.8840
			CF	9.7274	9.6773	9.6189	9.7643	9.7371	9.7090	9.7372	9.6960	9.6534
	100	0	SS	48.4892	48.2367	47.9289	48.6288	48.4680	48.2915	48.5299	48.3199	48.0953
			CC	153.4313	151.6762	149.4000	153.8780	152.4896	150.8894	153.6163	152.1272	150.4611
			CF	24.8321	24.7517	24.6538	24.8787	24.8289	24.7744	24.8454	24.7788	24.7076
	100	10	SS	58.5012	58.2487	57.9408	58.6408	58.4800	58.3035	58.5418	58.3319	58.1073
			CC	163.4751	161.7197	159.4431	163.9218	162.5330	160.9325	163.6601	162.1707	160.5044
			CF	34.8323	34.7519	34.6540	34.8789	34.8291	34.7745	34.8456	34.7790	34.7077

Table 13 Variation of nondimensional critical buckling loads of type B beam under different BCs, porosity distribution, and elastic foundation (1–2–1, $p = 2$)

L/h	K_w	K_p	BCs	e_0								
				UD			SD			ASD		
				0.4	0.6	0.8	0.4	0.6	0.4	0.4	0.6	0.8
5	0	0	SS	18.4506	17.6257	16.5807	18.5452	17.8365	17.0511	18.2592	17.4208	16.5241
			CC	59.8978	56.0151	51.0623	60.1714	56.7830	53.0390	60.1542	56.9359	53.5406
			CF	4.8809	4.6959	4.4660	4.9071	4.7497	4.5771	4.8081	4.5997	4.3758
	100	0	SS	28.6858	27.8578	26.8086	28.7794	28.0674	27.2782	28.4918	27.6494	26.7483
			CC	67.4569	63.5434	58.5418	67.7295	64.3137	60.5347	67.7211	64.4838	61.0665
			CF	16.3614	15.9043	15.2968	16.4155	16.0277	15.5820	16.2999	15.8621	15.3788
	100	10	SS	38.7805	37.9494	36.8958	38.8732	38.1579	37.3650	38.5841	37.7376	36.8321
			CC	77.6037	73.6822	68.6692	77.8747	74.4511	70.6629	77.8667	74.6224	71.1974
			CF	25.8352	25.3610	24.7316	25.9020	25.5068	25.0532	25.7920	25.3501	24.8626
20	0	0	SS	19.8405	19.1280	18.2492	19.9477	19.3434	18.6835	19.5178	18.6859	17.7913
			CC	78.3233	75.3566	71.6690	78.7403	76.2150	73.4450	77.1440	73.7950	70.1984
			CF	4.9830	4.8062	4.5887	5.0099	4.8601	4.6968	4.9003	4.6921	4.4681
	100	0	SS	29.9807	29.2681	28.3890	30.0878	29.4834	28.8233	29.6577	28.8256	27.9307
			CC	85.8880	82.9190	79.2280	86.3051	83.7778	81.0054	84.7082	81.3570	77.7577
			CF	17.7433	17.4009	16.9655	17.7937	17.5048	17.1817	17.5925	17.1898	16.7433
	100	10	SS	39.9887	39.2759	38.3966	40.0957	39.4911	38.8308	39.6655	38.8331	37.9378
			CC	95.9180	92.9484	89.2566	96.3349	93.8069	91.0336	94.7374	91.3851	87.7847
			CF	27.7428	27.4003	26.9649	27.7932	27.5042	27.1811	27.5919	27.1893	26.7428

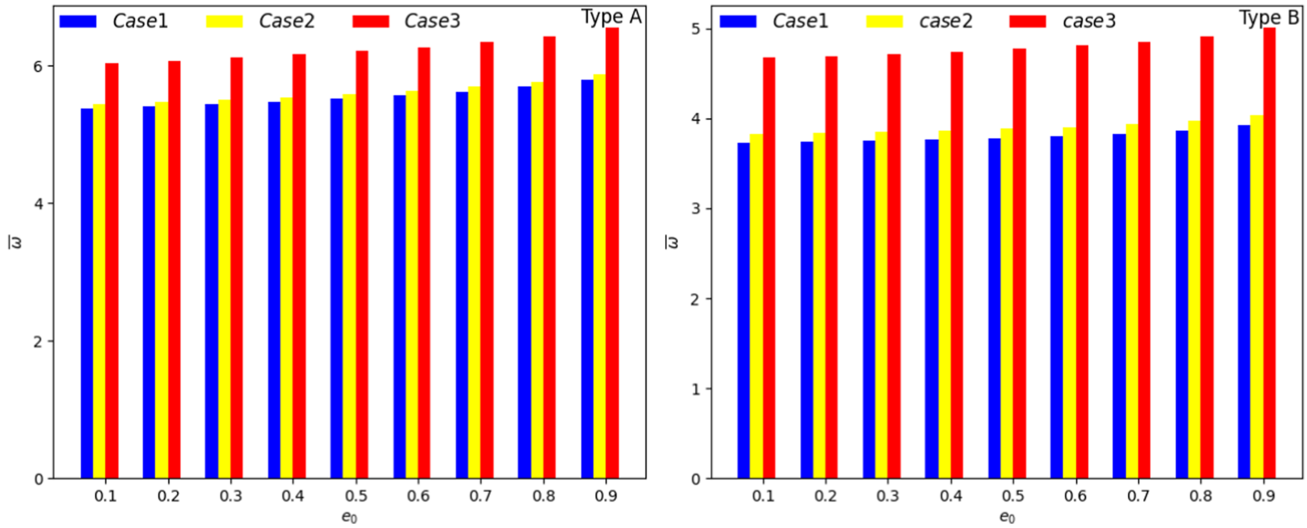

Fig. 4 The effect of porosity coefficient on fundamental natural frequencies of simple supported FG sandwich beams for symmetric porosity distribution and different elastic foundation constants (1–2–1, $L/h = 10$, $p = 5$)

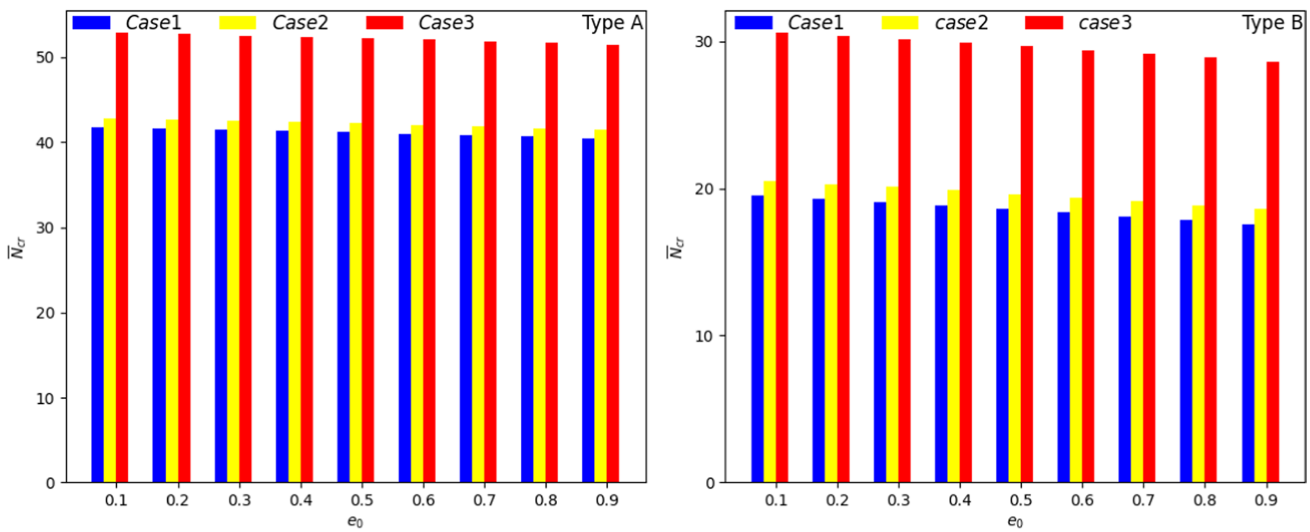

Fig. 5 The effect of porosity coefficient critical buckling loads of simply supported FG sandwich beams for symmetric porosity distribution and different elastic foundation constants (1–2–1, $L/h = 10$, $p = 5$)

there is a decrease observed for all cases as the porosity coefficient increases. In Case 2 introduction of the Winkler parameter (K_w) results in a slight increase in the fundamental natural frequencies and critical buckling loads of the beams. This phenomenon can be attributed to the stiffness of the Winkler foundation, which provides additional support and stability to the beams. Conversely, in case 3 the inclusion of the Pasternak parameter (K_p) leads to a significant enhancement in the fundamental natural frequencies and critical buckling loads effect by increasing the shear stiffness of the beams, resulting in a significant improvement in its free vibration and buckling behaviors. This observation suggests that the effect of the Pasternak parameter on both the natural frequency and critical buckling load is considerably more significant than the Winkler parameter.

4.3 Effect of Skin–Core-Skin Thickness Ratio

Tables 14 and 15 illustrate the effect of the skin–core-skin thickness ratio on the nondimensional fundamental natural frequencies and critical buckling loads for $L/h = 5$ and $p = 5$ with respect to the variation of the porosity coefficient of the three porosity patterns. It is, generally, noticeable that the nondimensional fundamental natural frequencies experience a decrease as the skin–core-skin thickness ratio decreases for Type A whereas an increase for Type B. This behavior can

Table 14 Variation of nondimensional fundamental natural frequencies of FG sandwich beams with different skin–core-skin thickness ratio, BCs, and porosity distribution ($L/h = 5$, $p = 5$, $K_w = 25$, $K_p = 10$)

Type	Scheme	BCs	UD			SD			ASD		
			0.4	0.6	0.8	0.4	0.6	0.8	0.4	0.6	0.8
Type A	2–1–2	SS	5.9176	5.9522	5.9994	5.9183	5.9540	6.0032	5.9182	5.9538	6.0030
		CC	9.9416	9.9719	10.0185	9.9443	9.9798	10.0376	9.9447	9.9804	10.0384
		CF	2.8424	2.8607	2.8853	2.8426	2.8611	2.8863	2.8425	2.8610	2.8862
	1–1–1	SS	5.8948	5.9497	6.0265	5.8966	5.9542	6.0369	5.8963	5.9538	6.0365
		CC	9.5034	9.5298	9.5780	9.5068	9.5438	9.6180	9.5098	9.5488	9.6251
		CF	2.8696	2.9006	2.9434	2.8702	2.9019	2.9463	2.8700	2.9017	2.9461
	1–2–1	SS	5.7687	5.8389	5.9394	5.7714	5.8470	5.9621	5.7721	5.8489	5.9663
		CC	8.8098	8.7901	8.7808	8.8039	8.7989	8.8397	8.8207	8.8273	8.8830
		CF	2.8759	2.9215	2.9859	2.8769	2.9242	2.9929	2.8769	2.9244	2.9936
Type B	2–1–2	SS	4.6028	4.6256	4.6583	4.6047	4.6299	4.6670	4.6015	4.6250	4.6602
		CC	7.8460	7.8566	7.8781	7.8586	7.8811	7.9233	7.8588	7.8816	7.9239
		CF	2.5083	2.5247	2.5473	2.5085	2.5253	2.5489	2.5073	2.5235	2.5463
	1–1–1	SS	4.6360	4.6732	4.7275	4.6395	4.6813	4.7452	4.6278	4.6634	4.7202
		CC	7.7560	7.7604	7.7776	7.7783	7.8063	7.8674	7.7716	7.7971	7.8559
		CF	2.5381	2.5660	2.6052	2.5385	2.5674	2.6089	2.5348	2.5616	2.6007
	1–2–1	SS	4.6783	4.7297	4.8074	4.6876	4.7491	4.8472	4.6573	4.7017	4.7806
		CC	7.6233	7.5999	7.5789	7.6582	7.6761	7.7404	7.8588	7.8816	7.9239
		CF	2.5765	2.6189	2.6798	2.5782	2.6228	2.6892	2.5692	2.6087	2.6692

Table 15 Variation of nondimensional critical buckling loads of FG sandwich beams with different skin–core skin thickness ratio, BCs, and porosity distribution ($L/h = 5$, $p = 5$, $K_w = 25$, $K_p = 10$)

Type	Scheme	BCs	UD			SD			USD		
			0.4	0.6	0.8	0.4	0.6	0.8	0.4	0.6	0.8
Type A	2–1–2	SS	56.8269	56.6839	56.5161	56.8413	56.7191	56.5936	56.8388	56.7155	56.5889
		CC	135.4088	134.3620	133.1466	135.4787	134.5662	133.6370	135.4890	134.5824	133.6594
		CF	26.4163	26.4006	26.3821	26.4193	26.4066	26.3935	26.4179	26.4045	26.3906
	1–1–1	SS	53.1604	52.7988	52.3617	53.1942	52.8839	52.5559	53.1893	52.8782	52.5506
		CC	117.4725	115.2651	112.6524	117.5501	115.5901	113.5595	117.6260	115.7107	113.7298
		CF	25.6836	25.6370	25.5808	25.6945	25.6578	25.6189	25.6886	25.6491	25.6074
	1–2–1	SS	47.0380	46.2146	45.1619	47.0797	46.3450	45.5223	47.0949	46.3838	45.5997
		CC	94.1891	90.1149	85.1373	94.0521	90.2651	86.2193	94.4120	90.8544	87.0772
		CF	24.2278	24.1003	23.9372	24.2568	24.1546	24.0390	24.2407	24.1324	24.0126
Type B	2–1–2	SS	31.5345	31.3267	31.0817	31.5833	31.4221	31.2567	31.5547	31.3798	31.2013
		CC	75.3644	74.3543	73.1665	75.6465	74.8854	74.1067	75.6709	74.9286	74.1734
		CF	18.8196	18.7665	18.7036	18.8317	18.7903	18.7476	18.8215	18.7751	18.7276
	1–1–1	SS	30.8751	30.4833	30.0093	30.9621	30.6571	30.3379	30.8311	30.4614	30.0787
		CC	71.2980	69.4067	67.1228	71.7706	70.3307	68.8293	71.6620	70.1924	68.6814
		CF	18.6597	18.5574	18.4330	18.6831	18.6037	18.5203	18.6400	18.5387	18.4331
	1–2–1	SS	30.0065	29.2949	28.4110	30.1896	29.6437	29.0563	29.8378	29.1160	28.3559
		CC	66.0736	62.8283	58.7845	66.7802	64.2465	61.5288	75.6709	74.9286	74.1734
		CF	18.4343	18.2392	17.9945	18.4915	18.3462	18.1887	18.3751	18.1682	17.9472

be attributed to the decrease in the beam's bending stiffness for Type A and the enhancement of the bending stiffness of the beam for Type B as the porous core thickness increases. The results indicate that the skin–core-skin thickness ratios 2–1–2 and 1–2–1 exhibit the lowest and highest values of the fundamental natural frequencies for Type A and reversely for Type B. However, for clamped Type B beams, the fundamental natural frequencies decrease as the skin–core-skin thickness ratio decreases for all types of porosity. Due to a relatively small length-to-thickness ratio $L/h = 5$ and an

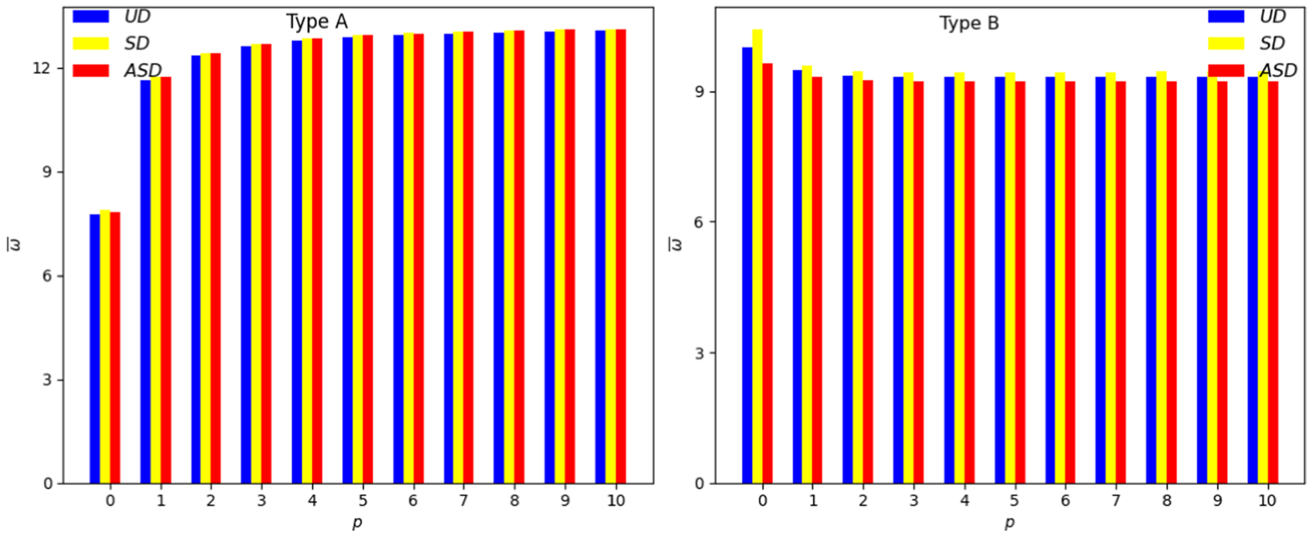

Fig. 6 Variation of nondimensional fundamental natural frequencies of clamped FG sandwich beams with the power index for different porosity distribution types (1–2–1, $L/h = 15$, $e_0 = 0.8$, $K_w = 50$, $K_p = 10$)

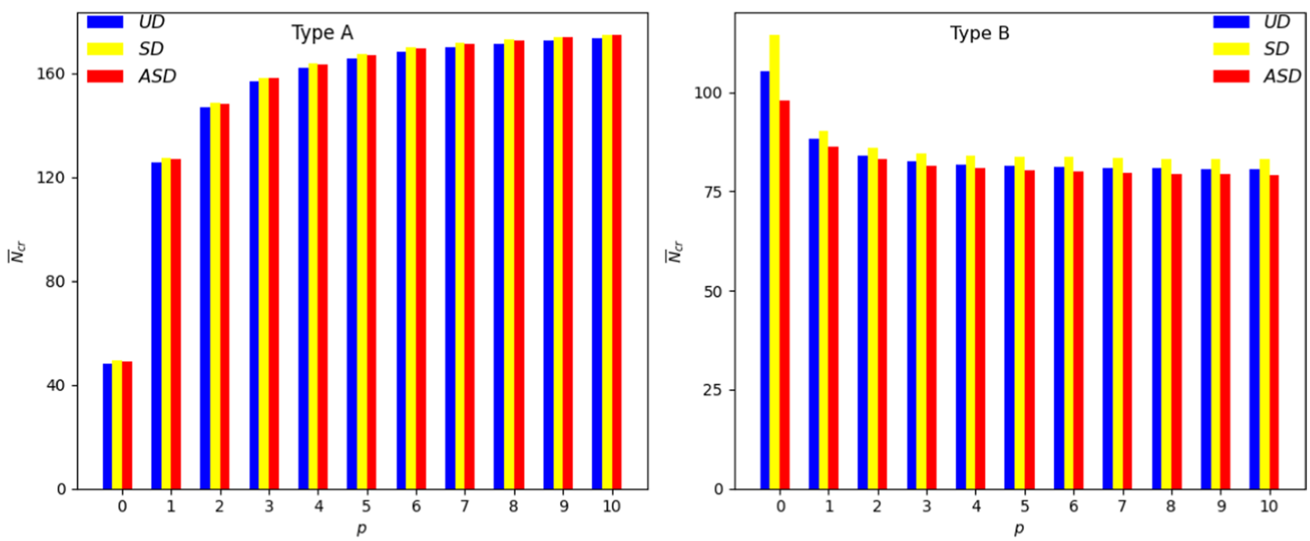

Fig. 7 Variation of nondimensional critical buckling loads of clamped FG sandwich beams with the power index for different porosity distribution types (1–2–1, $L/h = 15$, $e_0 = 0.8$, $K_w = 50$, $K_p = 10$)

FG core, the reduction rate in bending stiffness is more significant than the mass density for a CC beam. As a result, there is a decrease in the natural frequency as the thickness of the FG porous core increases. Similarly, the nondimensional critical buckling loads show a consistent decrease as the skin–core-skin thickness ratio decreases for both types. The results showcased in the tables emphasize the critical importance of carefully considering the geometric configurations, when designing FG sandwich beams with porous core to align with the desired performance criteria.

4.4 Effect of Power Index and Length-to-Thickness Ratio

Figures 6 and 7 illustrate the effect of the power index on the fundamental natural frequencies and critical buckling loads of FG sandwich beams with the three different porosity distribution patterns. A CC beam (1–2–1, $L/h = 15$, $e_0 = 0.8$, $K_w = 50$, $K_p = 10$) is considered. As expected, the nondimensional fundamental natural frequencies and critical buckling loads of FG sandwich beams increase with the power index for Type A, while for Type B, they

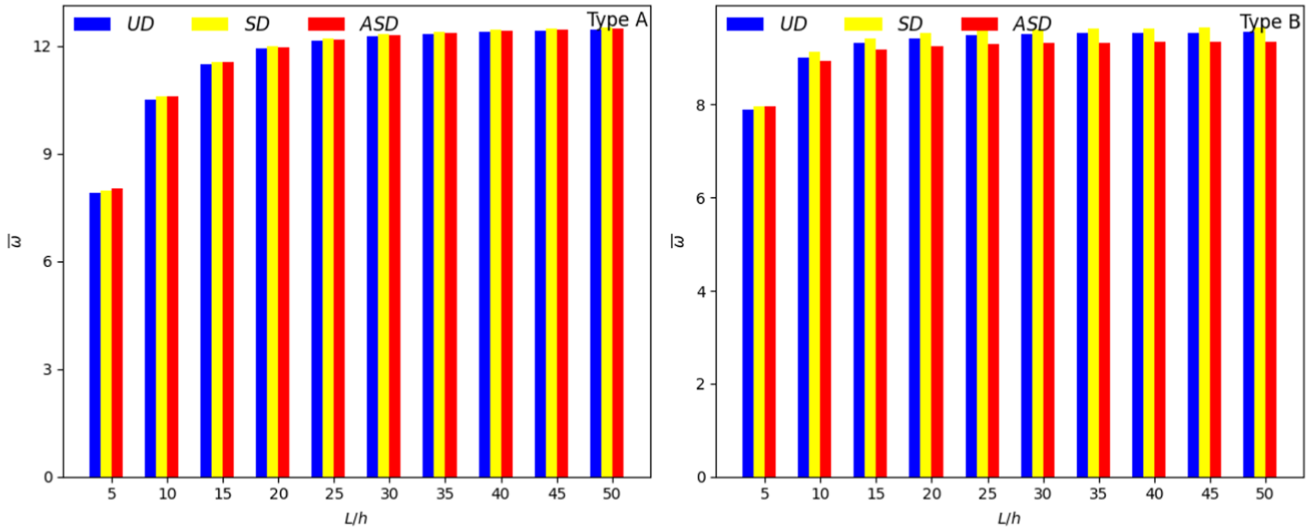

Fig. 8 Variation of nondimensional fundamental natural frequencies of clamped FG sandwich beams with the length-to-thickness ratio for different porosity distribution types (1–2–1, $e_0 = 0.8$, $K_w = K_p = 10$, $p = 1$)

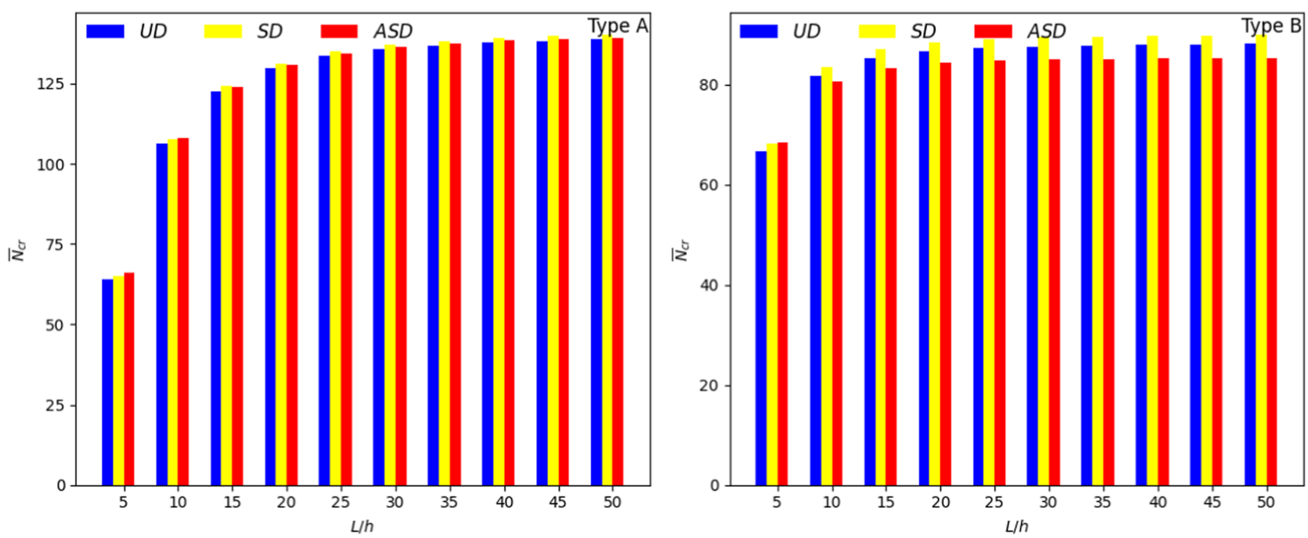

Fig. 9 Variation of nondimensional critical buckling loads of clamped–clamped FG sandwich beams with the length-to-thickness ratio for different porosity distribution types (1–2–1, $e_0 = 0.8$, $K_w = K_p = 10$, $p = 1$)

decrease inversely for all porosity distributions. It is seen that the effect of porosity distributions on nondimensional fundamental natural frequencies and critical buckling loads of Type A is relatively small compared to that observed for Type B beams. This smaller variation in natural frequencies and buckling loads for Type A beam with different porosity distributions can be attributed to the presence of FG face layers, which contribute significantly to the overall stiffness and dynamic properties of the beam, thereby reducing the relative impact of porosity distribution in the isotropic metal core. Conversely, in Type B the porosity distribution in the FG porous core has a more pronounced influence on the overall stiffness and natural frequencies than isotropic homogeneous face layers. However, the symmetric porosity distribution generally yields higher natural frequencies in both types. This is because a symmetric porosity distribution leads to a more uniform stiffness distribution along the beam's length, resulting in higher overall stiffness and natural frequencies. This highlights the importance of carefully considering the porosity distribution during the

Table 16 Variation of nondimensional fundamental natural frequencies of FG sandwich beams with various foundation parameters, BCs, and porosity distribution types (1–2–1, $L/h = 5$, $e_0 = 0.5$, $p = 5$)

Type	K_p	BCs	UD			SD			USD		
			K_w								
			0	50	100	0	50	100	0	50	100
Type A	0	SS	5.3099	5.6480	4.9543	5.3152	5.6530	4.9558	5.3165	5.6542	5.3099
		CC	8.4438	8.6636	8.2168	8.4426	8.6624	8.2407	8.4657	8.6850	8.4438
		CF	2.7118	3.3293	1.9067	2.7139	3.3309	1.9056	2.7132	3.3304	2.7118
	10	SS	5.9589	6.2620	5.6444	5.9636	6.2665	5.6456	5.9647	6.2675	5.9589
		CC	8.9056	9.1143	8.6908	8.9045	9.1132	8.7133	8.9265	9.1347	8.9056
		CF	3.2036	3.7420	2.5561	3.2051	3.7432	2.5561	3.2052	3.7433	3.2036
	25	SS	6.8174	7.0839	6.5443	6.8215	7.0878	6.5453	6.8224	7.0887	6.8174
		CC	9.5513	9.7462	9.3513	9.5503	9.7452	9.3724	9.5709	9.7654	9.5513
		CF	3.7502	4.2203	3.2133	3.7513	4.2212	3.2142	3.7520	4.2219	3.7502
Type B	0	SS	4.0608	4.5058	3.5821	4.0784	4.5205	3.5336	4.0350	4.4805	4.0608
		CC	7.1598	7.4247	6.9439	7.2159	7.4780	6.9180	7.1903	7.4525	7.1598
		CF	2.3701	3.0805	1.3279	2.3720	3.0803	1.3070	2.3590	3.0692	2.3701
	10	SS	4.9004	5.2749	4.5095	4.9128	5.2854	4.4695	4.8754	5.2500	4.9004
		CC	7.7375	7.9833	7.5372	7.7886	8.0321	7.5140	7.7655	8.0090	7.7375
		CF	2.9471	3.5461	2.1940	2.9485	3.5458	2.1811	2.9378	3.5360	2.9471
	25	SS	5.9408	6.2531	5.6201	5.9484	6.2595	5.5862	5.9158	6.2279	5.9408
		CC	8.5195	8.7435	8.3368	8.5649	8.7870	8.3166	8.5446	8.7666	8.5195
		CF	3.5359	4.0500	2.9367	3.5375	4.0500	2.9259	3.5276	4.0406	3.5359

Table 17 Variation of nondimensional critical buckling loads of FG sandwich beams with various foundation parameters, BCs, and porosity distribution types (1–2–1, $L/h = 5$, $e_0 = 0.5$, $p = 5$)

Type	K_p	BCs	UD			SD			USD		
			K_w								
			0	50	100	0	50	100	0	50	100
Type A	0	SS	33.9500	39.0830	44.2148	34.0264	39.1592	44.2908	34.0511	39.1842	44.3160
		CC	80.1628	83.9512	87.5819	80.1216	83.9092	87.5385	80.5894	84.3789	88.0124
		CF	10.2220	17.8497	23.1496	10.2603	17.8886	23.1901	10.2401	17.8744	23.1881
	10	SS	44.0809	49.2115	54.3409	44.1570	49.2874	54.4166	44.1822	49.3129	54.4424
		CC	90.3208	94.1052	97.7289	90.2787	94.0623	97.6847	90.7481	94.5335	98.1601
		CF	20.0995	27.5432	32.6499	20.1387	27.5848	32.6952	20.1179	27.5692	32.6904
	25	SS	59.2684	64.3954	69.5212	59.3441	64.4709	69.5966	59.3700	64.4971	69.6230
		CC	105.5231	109.2997	112.9106	105.4798	109.2556	112.8654	105.9513	109.7290	113.3430
		CF	34.6672	41.6901	46.3677	34.7106	41.7415	46.4295	34.6873	41.7206	46.4152
Type B	0	SS	17.0137	22.1291	27.2427	17.2699	22.3852	27.4987	16.8328	21.9469	27.0592
		CC	52.4637	56.2649	59.9517	53.4780	57.2808	60.9735	53.0624	56.8674	60.5678
		CF	4.5804	11.5471	15.5345	4.6427	11.6435	15.6848	4.4981	11.4807	15.4884
	10	SS	27.1094	32.2212	37.3312	27.3653	32.4771	37.5870	26.9259	32.0365	37.1453
		CC	62.6092	66.4031	70.0810	63.6235	67.4192	71.1031	63.2076	67.0054	70.6973
		CF	14.4741	21.2031	24.9816	14.5391	21.3102	25.1488	14.3960	21.1506	24.9587
	25	SS	42.2396	47.3460	52.4507	42.4954	47.6019	52.7065	42.0525	47.1578	52.2613
		CC	77.7772	81.5581	85.2201	78.7923	82.5753	86.2439	78.3759	82.1611	85.8379
		CF	28.9777	35.0850	38.3594	29.0603	35.2385	38.5931	28.9202	35.0842	38.4153

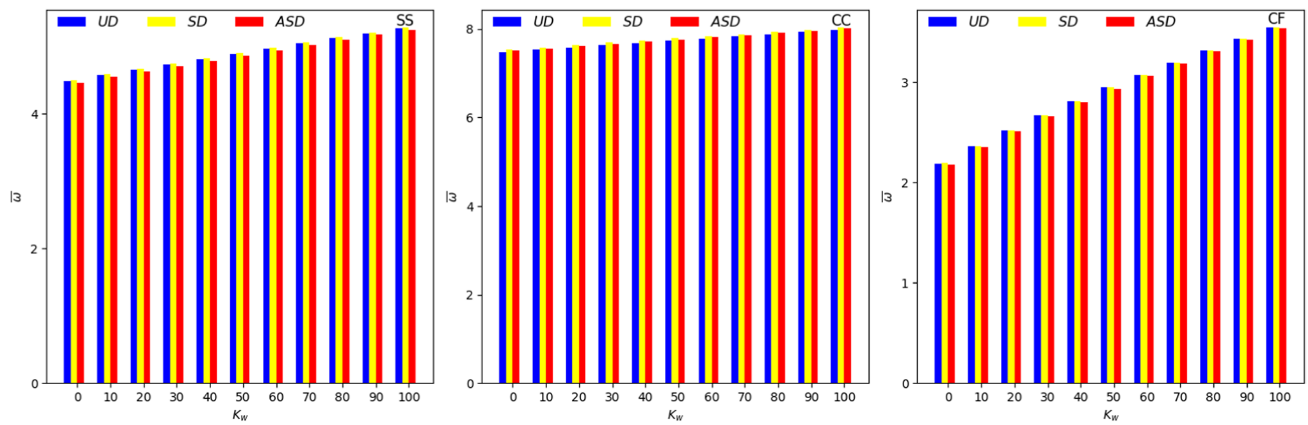

(a) with respect to K_w ($K_p = 10$)

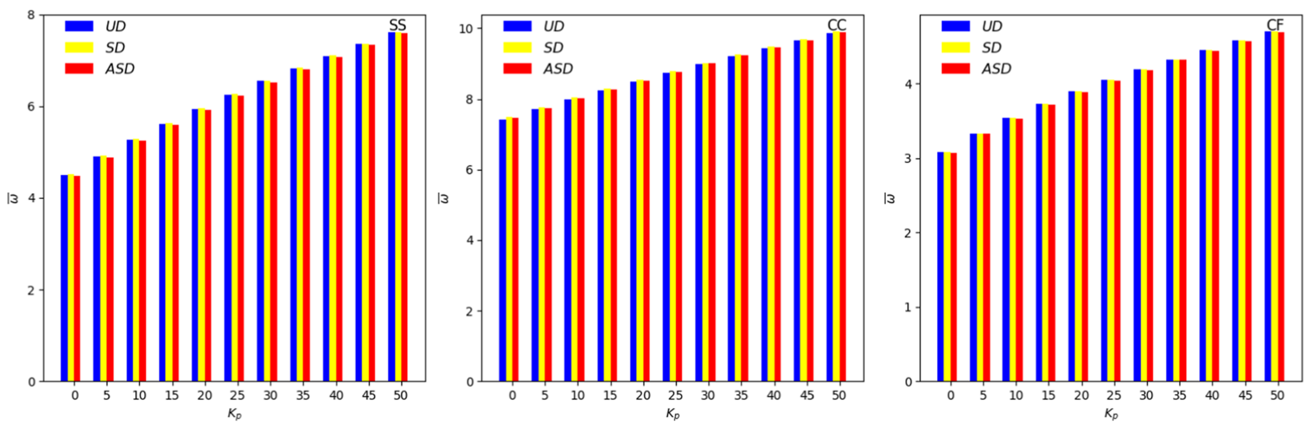

(b) with respect to K_p ($K_w = 100$)

Fig. 10 Variation of nondimensional fundamental natural frequencies of Type B for various BCs and porosity distributions (1–2–1, $L/h = 5$, $e_0 = 0.8$, $p = 5$) under K_w and K_p

manufacturing process. Optimization of porosity distribution can lead to achieve desired mechanical performance of the beams while ensuring cost-effectiveness and feasibility during the design and manufacturing process.

Figures 8 and 9 demonstrate the effect of length-to-thickness ratio L/h on the fundamental natural frequencies and critical buckling loads of FG sandwich beams with the three porosity distribution patterns. A CC beam (1–2–1, $e_0 = 0.8$, $K_w = K_p = 10$, $p = 1$) is considered. It is seen that the nondimensional fundamental natural frequencies and critical buckling loads of FG sandwich beam increase as the increase of length-to-thickness ratio L/h for all porosity distributions. Moreover, the difference in nondimensional fundamental natural frequencies and critical buckling loads for porosity distribution patterns becomes significant as the length-to-thickness ratio increases. This is because, with higher length-to-thickness ratios, porosity has a more significant impact on the overall stiffness and mechanical behavior of the beam. The findings illustrated that incorporating porosity can effectively lead to a reduction in overall material density while still maintaining adequate stiffness and buckling resistance, particularly evident in beams with higher L/h ratios. This implies that for applications where weight reduction is a priority, the use of porous core materials in FG sandwich beams with higher L/h ratios can be advantageous.

4.5 Effect of Elastic Foundation

To study the effects of foundation parameters with different porosity patterns and BCs on free vibration and buckling behavior of 1–2–1 sandwich beam with $L/h = 5$, $e_0 = 0.5$, $p = 5$ are considered. The variation of nondimensional fundamental natural frequencies and critical buckling loads with different foundation parameters, porosity patterns, and BCs are summarized in Tables 16 and 17. It is seen that the nondimensional fundamental frequencies and critical buckling loads increase with the enhancement of foundation parameters for all porosity distributions and BCs. This behavior

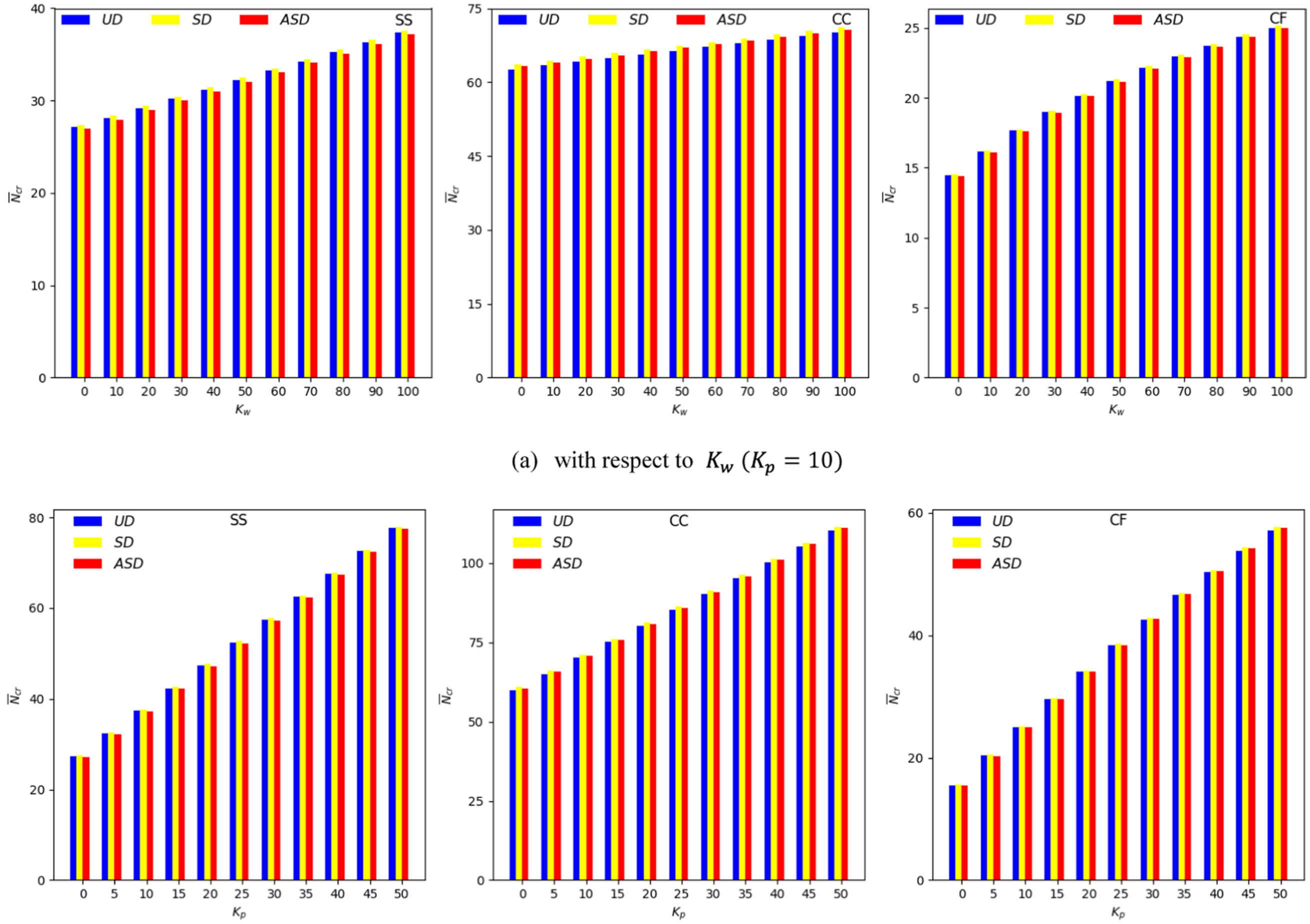

(a) with respect to K_w $(K_p = 10)$

(b) with respect to K_p $(K_w = 100)$

Fig. 11 Variation of nondimensional critical buckling loads of Type B for various BCs and porosity distributions (1–2–1, $L/h = 5$, $e_0 = 0.8$, $p = 5$) under K_w and K_p

is attributed to the fact that increasing the elastic foundation parameter amplifies the bending stiffness of the beam, thereby improving its vibrational and buckling resistance.

Figures 10 and 11 show the variations of nondimensional fundamental natural frequencies and critical buckling loads as a function of elastic foundation parameters to evaluate separately the effects of Winkler and Pasternak elastic foundation parameters. It should be noted that the nondimensional fundamental natural frequencies and critical buckling loads increase considerably with the increase of the Pasternak parameter. From this, it can be inferred that changes in K_p have a more pronounced impact on fundamental frequencies and critical buckling loads compared to changes in K_w. Besides, the effect of porosity distribution patterns is found to be negligible, especially for the CF beam. This is primarily attributed to the fact that the elastic foundation has a more significant effect on the bending stiffness than the porosity effect.

5 Conclusion

This paper presented a new finite element model based on quasi-3D deformation theory for free vibration and buckling analysis of FG sandwich beams with porous core resting on a two-parameter Winkler-Pasternak elastic foundation. Three different porosity patterns including uniform, symmetric, and asymmetric are considered. A three-nodded finite element having 15-DOFs is proposed for the numerical solution. The accuracy and convergence of the proposed model is verified with several examples. A comprehensive parametric study is carried out to explore the effects of the boundary conditions, skin-to-core thickness ratio, power-law index, slenderness, porosity, and elastic foundation parameters on the natural frequencies and critical buckling loads of FG sandwich beams. The main findings from the study can be summarized as follows:

1. For FG sandwich beams with a porous metal core, the fundamental natural frequencies and critical buckling loads increase with the increase of the power-law index and inversely they decrease with the power-law index for sandwich beams with FG core.
2. As the porosity coefficient increases, the fundamental natural frequencies increase, while the critical buckling loads decrease due to the concurrent reduction in the bending stiffness and mass density.
3. Symmetric porosity distribution yields the most favorable fundamental natural frequencies and critical buckling loads.
4. As the skin–core-skin thickness ratio decreases, the fundamental natural frequencies decrease for Type A and increase for Type B. Critical buckling loads decrease for both types.
5. An increase in the length-to-thickness ratio results in higher fundamental natural frequencies and critical buckling loads for FG sandwich beams and the porosity distribution effect becomes more significant.
6. The fundamental natural frequencies and critical buckling loads of the FG sandwich beam increase significantly as the spring and shear constants of the elastic foundation increase, particularly when the shear layer constant increases.

Appendix

The shape functions $\psi_i(x)$ and $\varphi_i(x)$ are given are given as follows:

$$
\begin{aligned}
&\psi_1 = 1 - \frac{3x}{L} + 2\left(\frac{x}{L}\right)^2, \quad \psi_2 = \frac{4x}{L} - \frac{4x^2}{L^2}, \\
&\psi_3 = -\frac{x}{L} + 2\left(\frac{x}{L}\right)^2, \\
&\varphi_1 = 1 - \frac{23x^2}{L^2} + \frac{66x^3}{L^3} - \frac{68x^4}{L^4} + \frac{24x^5}{L^5}, \\
&\varphi_2 = x - \frac{6x^2}{L} + \frac{13x^3}{L^2} - \frac{12x^4}{L^3} + \frac{4x^5}{L^4}, \\
&\varphi_3 = \frac{16x^2}{L^2} - \frac{32x^3}{L^3} + \frac{16x^4}{L^4}, \\
&\varphi_4 = -\frac{8x^2}{L} + \frac{32x^3}{L^2} - \frac{40x^4}{L^3} + \frac{16x^5}{L^4}, \\
&\varphi_5 = \frac{7x^2}{L^2} - \frac{34x^3}{L^3} + \frac{52x^4}{L^4} - \frac{24x^5}{L^5}, \\
&\varphi_6 = -\frac{x^2}{L} + \frac{5x^3}{L^2} - \frac{8x^4}{L^3} + \frac{4x^5}{L^4}
\end{aligned}
\tag{A1}
$$

The components of the stiffness matrix K and the mass matrix M are given as follows:

$$
\begin{aligned}
&\mathbf{K} = \begin{bmatrix} K_{11}K_{12}K_{13}K_{14} \\ K_{12}K_{22}K_{23}K_{24} \\ K_{13}K_{23}K_{33}K_{34} \\ K_{14}K_{24}K_{34}K_{44} \end{bmatrix}, \mathbf{M} = \begin{bmatrix} M_{11}M_{12}M_{13}M_{14} \\ M_{12}M_{22}M_{23}M_{24} \\ M_{13}M_{23}M_{33}M_{34} \\ M_{14}M_{24}M_{34}M_{44} \end{bmatrix}, \\
&\boldsymbol{G} = \begin{bmatrix} 0 & 0 & 0\,0 \\ 0 & N_{22} & 0\,0 \\ 0 & 0 & 0\,0 \\ 0 & 0 & 0\,0 \end{bmatrix}, \quad \boldsymbol{\Delta} = \begin{Bmatrix} u_i \\ w_i \\ \phi_{yi} \\ \phi_{zi} \end{Bmatrix}
\end{aligned}
\tag{A2}
$$

where

$$
\begin{aligned}
&K_{11}(i,j) = A_{11}\int_0^L \psi_{i,x}\psi_{j,x}\mathrm{d}x, K_{12}(i,j) = -B_{11}\int_0^L \psi_{i,x}\varphi_{j,xx}\mathrm{d}x,\\
&K_{13}(i,j) = C_{11}\int_0^L \psi_{i,x}\psi_{j,x}\mathrm{d}x, K_{14}(i,j) = B_{S13}\int_0^L \psi_{i,x}\psi_{j}\mathrm{d}x,\\
&K_{22}(i,j) = E_{11}\int_0^L \varphi_{i,xx}\varphi_{j,xx}\mathrm{d}x - N_0\int_0^L \varphi_{i,x}\varphi_{j,x}\mathrm{d}x\\
&\quad + k_w\int_0^L \varphi_i\varphi_j dx + k_p\int_0^L \varphi_{i,x}\varphi_{j,x}\mathrm{d}x,\\
&K_{23}(i,j) = -D_{11}\int_0^L \varphi_{i,xx}\psi_{j,x}\mathrm{d}x,\\
&K_{24}(i,j) = -C_{S13}\int_0^L \varphi_{i,xx}\psi_{j}\mathrm{d}x + gk_w\int_0^L \varphi_i\psi_j\mathrm{d}x\\
&\quad + gk_p\int_0^L \varphi_{i,x}\psi_{j,x}\mathrm{d}x,\\
&K_{33}(i,j) = F_{11}\int_0^L \psi_{i,x}\psi_{j,x}\mathrm{d}x + A_{s55}\int_0^L \psi_i\psi_j\mathrm{d}x,\\
&K_{34}(i,j) = E_{S13}\int_0^L \psi_{i,x}\psi_{j}\mathrm{d}x + A_{s55}\int_0^L \psi_i\psi_{j,x}\mathrm{d}x,\\
&K_{44}(i,j) = D_{S33}\int_0^L \psi_i\psi_j\mathrm{d}x + A_{s55}\int_0^L \psi_{i,x}\psi_{j,x}\mathrm{d}x\\
&\quad + g^2k_w\int_0^L \psi_i\psi_j\mathrm{d}x + g^2k_p\int_0^L \psi_{i,x}\psi_{j,x}\mathrm{d}x,\\
&M_{11}(i,j) = I_1\int_0^L \psi_i\psi_j\mathrm{d}x, M_{12}(i,j) = -I_2\int_0^L \psi_i\varphi_{j,x}\mathrm{d}x,\\
&\quad M_{13}(i,j) = I_4\int_0^L \psi_i\psi_j\mathrm{d}x, M_{14}(i,j) = 0,\\
&M_{22}(i,j) = I_1\int_0^L \varphi_i\varphi_j\mathrm{d}x + I_3\int_0^L \varphi_{i,x}\varphi_{j,x}\mathrm{d}x,\\
&\quad M_{23}(i,j) = -I_5\int_0^L \varphi_{i,x}\psi_j\mathrm{d}x, M_{24}(i,j) = I_7\int_0^L \varphi_i\psi_j\mathrm{d}x,\\
&M_{33}(i,j) = I_6\int_0^L \psi_i\psi_j\mathrm{d}x, M_{34}(i,j) = 0, M_{44}(i,j) = I_8\\
&\quad \int_0^L \psi_i\psi_j\mathrm{d}x, N_{22}(i,j) = N_0\int_0^L \varphi_{i,x}\varphi_{j,x}\mathrm{d}x
\end{aligned}
\tag{A3}
$$

Author contributions All authors contributed to the study conception and design. Material preparation, data collection and analysis were performed by Ibrahim Mohamed and Volkan Kahya. The first draft of the manuscript was written by Ibrahim Mohamed and all authors commented on previous versions of the manuscript. All authors read and approved the final manuscript.

Declarations

Conflict of interest The author(s) declare that there are no potential conflicts of interest concerning the research, authorship, and/or publication of this article.

Ethical approval This article does not contain any studies with human participants or animals performed by any of the authors.

Replication of results Codes and data for replication can be provided upon request.

References

Ait Atmane H, Tounsi A, Bernard F (2017) Effect of thickness stretching and porosity on mechanical response of a functionally graded beams resting on elastic foundations. Int J Mech Mater Des 13:71–84. https://doi.org/10.1007/s10999-015-9318-x

Akbaş ŞD, Fageehi YA, Assie AE, Eltaher MA (2022) Dynamic analysis of viscoelastic functionally graded porous thick beams under pulse load. Eng Comput 38:365–377. https://doi.org/10.1007/s00366-020-01070-3

Alambeigi K, Mohammadimehr M, Bamdad M, Rabczuk T (2020) Free and forced vibration analysis of a sandwich beam considering porous core and SMA hybrid composite face layers on Vlasov's foundation. Acta Mech 231:3199–3218. https://doi.org/10.1007/s00707-020-02697-5

Al-Itbi SK, Noori AR (2022) Finite element analysis for the static response of functionally graded porous sandwich beams. Int J Eng Technol IJET 8:13–20. https://doi.org/10.19072/ijet.1161612

Arslan K, Gunes R (2018) Low-velocity flexural impact analyses of functionally graded sandwich beams using finite element modeling. Int J Appl Mech. https://doi.org/10.1142/S1758825118501132

Bamdad M, Mohammadimehr M, Alambeigi K (2019) Analysis of sandwich Timoshenko porous beam with temperature-dependent material properties: magneto-electro-elastic vibration and buckling solution. J Vib Control 25:2875–2893. https://doi.org/10.1177/1077546319860314

Bang S-O, Cho J-U (2015) A study on the compression property of sandwich composite with porous core. Int J Precis Eng Manuf 16:1117–1122. https://doi.org/10.1007/s12541-015-0144-8

Bargozini F, Mohammadimehr M, Dawi EA, Salavati-Niasari M (2024) Buckling of a sandwich beam with carbon nano rod reinforced composite and porous core under axially variable forces by considering general strain. Res Eng.https://doi.org/10.1016/j.rineng.2024.101945

Belarbi M-O, Houari MSA, Hirane H, Daikh AA, Bordas SPA (2022) On the finite element analysis of functionally graded sandwich curved beams via a new refined higher order shear deformation theory. Compos Struct 279:114715. https://doi.org/10.1016/j.compstruct.2021.114715

Betts C (2012) Benefits of metal foams and developments in modelling techniques to assess their materials behaviour: a review.

Mater Sci Technol 28:129–143. https://doi.org/10.1179/026708311X13135950699290
Chami GMB, Kahil A, Hadji L (2022) Influence of porosity on the fundamental natural frequencies of FG sandwich beams. Mater Today Proc 53:107–112. https://doi.org/10.1016/j.matpr.2021.12.404
Chen D, Yang J, Kitipornchai S (2015) Elastic buckling and static bending of shear deformable functionally graded porous beam. Compos Struct 133:54–61. https://doi.org/10.1016/j.compstruct.2015.07.052
Chen D, Kitipornchai S, Yang J (2016) Nonlinear free vibration of shear deformable sandwich beam with a functionally graded porous core. Thin-Walled Struct 107:39–48. https://doi.org/10.1016/j.tws.2016.05.025
Chinh TH, Tu TM, Duc DM, Hung TQ (2021) Static flexural analysis of sandwich beam with functionally graded face sheets and porous core via point interpolation meshfree method based on polynomial basic function. Arch Appl Mech 91:933–947. https://doi.org/10.1007/s00419-020-01797-x
Conde Y, Pollien A, Mortensen A (2006) Functional grading of metal foam cores for yield-limited lightweight sandwich beams. Scr Mater 54:539–543. https://doi.org/10.1016/j.scriptamat.2005.10.050
Derikvand M, Farhatnia F, Hodges DH (2023) Functionally graded thick sandwich beams with porous core: buckling analysis via differential transform method. Mech Based Des Struct Mach 51:3650–3677. https://doi.org/10.1080/15397734.2021.1931309
Eltaher MA, Fouda N, El-midany T, Sadoun AM (2018) Modified porosity model in analysis of functionally graded porous nanobeams. J Braz Soc Mech Sci Eng 40:141. https://doi.org/10.1007/s40430-018-1065-0
Fahsi B, Bouiadjra RB, Mahmoudi A, Benyoucef S, Tounsi A (2019) Assessing the effects of porosity on the bending, buckling, and vibrations of functionally graded beams resting on an elastic foundation by using a new refined quasi-3D theory. Mech Compos Mater 55:219–230. https://doi.org/10.1007/s11029-019-09805-0
Fazzolari FA (2018) Generalized exponential, polynomial and trigonometric theories for vibration and stability analysis of porous FG sandwich beams resting on elastic foundations. Compos B Eng 136:254–271. https://doi.org/10.1016/j.compositesb.2017.10.022
Foroutan K, Carrera E, Pagani A, Ahmadi H (2021) Post-buckling and large-deflection analysis of a sandwich FG plate with FG porous core using Carrera's Unified Formulation. Compos Struct. https://doi.org/10.1016/j.compstruct.2021.114189
Ghazwani MH, Alnujaie A, Van Vinh P, Civalek Ö (2024) High frequency analysis of the functionally graded sandwich nanobeams embedded in elastic foundations using nonlocal quasi-3D theory. Phys B Condens Matter. https://doi.org/10.1016/j.physb.2023.415646
Grygorowicz M, Magnucki K, Malinowski M (2015) Elastic buckling of a sandwich beam with variable mechanical properties of the core. Thin-Walled Struct 87:127–132. https://doi.org/10.1016/j.tws.2014.11.014
Gupta S, Chalak HD (2023) Buckling analysis of functionally graded sandwich beam based on third-order zigzag theory. Mech Adv Compos Struct 10:55–68. https://doi.org/10.22075/macs.2022.27831.1421
Hamed MA, Abo-bakr RM, Mohamed SA, Eltaher MA (2020) Influence of axial load function and optimization on static stability of sandwich functionally graded beams with porous core. Eng Comput 36:1929–1946. https://doi.org/10.1007/s00366-020-01023-w
Han X-H, Wang Q, Park Y-G, T'Joen C, Sommers A, Jacobi A (2012) A review of metal foam and metal matrix composites for heat exchangers and heat sinks. Heat Transfer Eng 33:991–1009. https://doi.org/10.1080/01457632.2012.659613
Hung DX, Truong HQ (2018) Free vibration analysis of sandwich beams with FG porous core and FGM faces resting on Winkler elastic foundation by various shear deformation theories. J Sci Technol Civil Eng (STCE)—NUCE 12:23–33. https://doi.org/10.31814/stce.nuce2018-12(3)-03
Kahya V, Turan M (2017) Finite element model for vibration and buckling of functionally graded beams based on the first-order shear deformation theory. Compos B Eng 109:108–115. https://doi.org/10.1016/j.compositesb.2016.10.039
Khaneh Masjedi P, Maheri A, Weaver PM (2019) Large deflection of functionally graded porous beams based on a geometrically exact theory with a fully intrinsic formulation. Appl Math Model 76:938–957. https://doi.org/10.1016/j.apm.2019.07.018
Koutoati K, Mohri F, Daya EM, Carrera E (2021a) A finite element approach for the static and vibration analyses of functionally graded material viscoelastic sandwich beams with nonlinear material behavior. Compos Struct. https://doi.org/10.1016/j.compstruct.2021.114315
Koutoati K, Mohri F, Daya EM (2021b) Finite element approach of axial bending coupling on static and vibration behaviors of functionally graded material sandwich beams. Mech Adv Mater Struct 28:1537–1553. https://doi.org/10.1080/15376494.2019.1685144
Lefebvre L-P, Banhart J, Dunand DC (2008) Porous metals and metallic foams: current status and recent developments. Adv Eng Mater 10:775–787. https://doi.org/10.1002/adem.200800241
Li C, Shen H-S, Yang J (2023) Nonlinear vibration behavior of FG sandwich beams with auxetic porous copper core in thermal environments. Int J Struct Stab Dyn. https://doi.org/10.1142/S0219455423501444
Madenci E, Özkılıç YO (2021) Free vibration analysis of open-cell FG porous beams: analytical, numerical and ANN approaches. Steel Compos Struct 40:157–173. https://doi.org/10.12989/scs.2021.40.2.157
Magnucka-Blandzi E, Magnucki K (2007) Effective design of a sandwich beam with a metal foam core. Thin-Walled Struct 45:432–438. https://doi.org/10.1016/j.tws.2007.03.005
Malhari Ramteke P, Mehar K, Sharma N, Panda S (2020) Numerical prediction of deflection and stress responses of functionally graded structure for grading patterns (Power-Law, Sigmoid and Exponential) and variable porosity (Even/Uneven). Scientia Iranica. https://doi.org/10.24200/sci.2020.55581.4290
Matinfar M, Shirazi MM, Alipour MM (2019) Analysis of bi-directional FG porous sandwich beams in hygrothermal environment resting on Winkler/Pasternak foundation, based on the layerwise theory and Chebyshev-Tau method. J Stress Anal. https://doi.org/10.22084/jrstan.2019.18781.1090
Mohammed AT, Hareb MA, Eqal AK (2021) Investigation on the Analysis of Bending and Buckling for FGM Euler-Bernoulli Beam Resting on Winkler-Pasternak Elastic Foundation. In: Journal of Physics: Conference Series. IOP Publishing Ltd
Nguyen T-K, Truong-Phong Nguyen T, Vo TP, Thai H-T (2015) Vibration and buckling analysis of functionally graded sandwich beams by a new higher-order shear deformation theory. Compos B Eng 76:273–285. https://doi.org/10.1016/j.compositesb.2015.02.032
Nguyen T-K, Vo TP, Nguyen B-D, Lee J (2016) An analytical solution for buckling and vibration analysis of functionally graded sandwich beams using a quasi-3D shear deformation theory. Compos Struct 156:238–252. https://doi.org/10.1016/j.compstruct.2015.11.074
Nguyen N-D, Nguyen T-N, Nguyen T-K, Vo TP (2022a) A new two-variable shear deformation theory for bending, free vibration and buckling analysis of functionally graded porous beams. Compos Struct 282:115095. https://doi.org/10.1016/j.compstruct.2021.115095
Nguyen VC, Tran TT, Nguyen-Thoi T, Pham QH (2022b) A novel finite element formulation for static bending analysis of functionally

graded porous sandwich plates. Front Struct Civ Eng 16:1599–1620. https://doi.org/10.1007/s11709-022-0891-4

Nguyen N-D, Nguyen T-N, Nguyen T-K, Vo TP (2023) A Legendre-Ritz solution for bending, buckling and free vibration behaviours of porous beams resting on the elastic foundation. Structures 50:1934–1950. https://doi.org/10.1016/j.istruc.2023.03.018

Nguyen Thi H (2022) On mechanical behavior of two-layer functionally graded sandwich curved beams resting on elastic foundations using an analytical solution and refined Timoshenko beam theory. Ain Shams Eng J. https://doi.org/10.1016/j.asej.2021.11.016

Patel P, Bhingole PP, Makwana D (2018) Manufacturing, characterization and applications of lightweight metallic foams for structural applications: review. Mater Today Proc 5:20391–20402. https://doi.org/10.1016/j.matpr.2018.06.414

Patil R, Joladarashi S, Kadoli R (2023) Bending and vibration studies of FG porous sandwich beam with viscoelastic boundary conditions: FE approach. Mech Adv Mater Struct 30:3588–3607. https://doi.org/10.1080/15376494.2022.2079030

Ramteke PM, Panda SK (2021) Free vibrational behaviour of multi-directional porous functionally graded structures. Arab J Sci Eng 46:7741–7756. https://doi.org/10.1007/s13369-021-05461-6

Reddy JN (1984) A simple higher order theory for laminated composite plates. ASME J Appl Mech 51:745–752

Sayyad AS, Avhad PV, Hadji L (2022) On the static deformation and frequency analysis of functionally graded porous circular beams. Forces in Mech 7:100093. https://doi.org/10.1016/j.finmec.2022.100093

Smith BH, Szyniszewski S, Hajjar JF, Schafer BW, Arwade SR (2012) Steel foam for structures: a review of applications, manufacturing and material properties. J Constr Steel Res 71:1–10. https://doi.org/10.1016/j.jcsr.2011.10.028

Songsuwan W, Pimsarn M, Wattanasakulpong N (2018) Dynamic responses of functionally graded sandwich beams resting on elastic foundation under harmonic moving loads. Int J Struct Stab Dyn. https://doi.org/10.1142/S0219455418501122

Srikarun B, Songsuwan W, Wattanasakulpong N (2021) Linear and nonlinear static bending of sandwich beams with functionally graded porous core under different distributed loads. Compos Struct 276:114538. https://doi.org/10.1016/j.compstruct.2021.114538

Su J, Xiang Y, Ke L-L, Wang Y-S (2019) Surface effect on static bending of functionally graded porous nanobeams based on Reddy's beam theory. Int J Struct Stab Dyn 19:1950062. https://doi.org/10.1142/S0219455419500627

Tang H, Li L, Hu Y (2018) Buckling analysis of two-directionally porous beam. Aerosp Sci Technol 78:471–479. https://doi.org/10.1016/j.ast.2018.04.045

Turan M, Adiyaman G (2023) A new higher-order finite element for static analysis of two-directional functionally graded porous beams. Arab J Sci Eng. https://doi.org/10.1007/s13369-023-07742-8

Turan M, Uzun Yaylacı E, Yaylacı M (2023) Free vibration and buckling of functionally graded porous beams using analytical, finite element, and artificial neural network methods. Arch Appl Mech 93:1351–1372. https://doi.org/10.1007/s00419-022-02332-w

Van Vinh P, Duoc NQ, Phuong ND (2022) A new enhanced first-order beam element based on neutral surface position for bending analysis of functionally graded porous beams. Iran J Sci Tech—Trans Mech Eng 46:1141–1156. https://doi.org/10.1007/s40997-022-00485-1

Van Vinh P, Belarbi MO, Avcar M, Civalek Ö (2023) An improved first-order mixed plate element for static bending and free vibration analysis of functionally graded sandwich plates. Arch Appl Mech 93:1841–1862. https://doi.org/10.1007/s00419-022-02359-z

Van VP (2022) Analysis of bi-directional functionally graded sandwich plates via higher-order shear deformation theory and finite element method. J Sandwich Struct Mater 24:860–899. https://doi.org/10.1177/10996362211025811

Vo TP, Thai H-T, Nguyen T-K, Maheri A, Lee J (2014) Finite element model for vibration and buckling of functionally graded sandwich beams based on a refined shear deformation theory. Eng Struct 64:12–22. https://doi.org/10.1016/j.engstruct.2014.01.029

Vo TP, Thai H-T, Nguyen T-K, Inam F, Lee J (2015) A quasi-3D theory for vibration and buckling of functionally graded sandwich beams. Compos Struct 119:1–12. https://doi.org/10.1016/j.compstruct.2014.08.006

Wattanasakulpong N, Ungbhakorn V (2014) Linear and nonlinear vibration analysis of elastically restrained ends FGM beams with porosities. Aerosp Sci Technol 32:111–120. https://doi.org/10.1016/j.ast.2013.12.002

Wu H, Yang J, Kitipornchai S (2020) Mechanical analysis of functionally graded porous structures: a review. Int J Struct Stab Dyn 20:2041015. https://doi.org/10.1142/S0219455420410151

Xin L, Kiani Y (2023) Vibration characteristics of arbitrary thick sandwich beam with metal foam core resting on elastic medium. Structures 49:1–11. https://doi.org/10.1016/j.istruc.2023.01.108

Zenkour A, Ebrahimi F, Barati MR (2019) Buckling analysis of a size-dependent functionally graded nanobeam resting on Pasternak's foundations. Int J Nano Dimens 10(2):141–153

Zghal S, Ataoui D, Dammak F (2022) Static bending analysis of beams made of functionally graded porous materials. Mech Based Des Struct Mach 50:1012–1029. https://doi.org/10.1080/15397734.2020.1748053